AGU PUBLICATIONS

Water Resources Research

RESEARCH ARTICLE
10.1002/2016WR019143

Modeling sediment mobilization using a distributed hydrological model coupled with a bank stability model

J. Stryker[1], B. Wemple[2], and A. Bomblies[1]

[1]School of Engineering, University of Vermont, Burlington, Vermont, USA, [2]Department of Geography, University of Vermont, Burlington, Vermont, USA

Key Points:
- Coupled model more inclusively represents suspended sediment mobilization in a watershed by including stream bank erosion and failure
- Modeled sediment using new approach improves suspended sediment representation at high flows in a test watershed
- Inclusive modeling of sediment mobilization will be important for simulating watershed response to climate shifts and land use change

Supporting Information:
- Supporting Information S1

Correspondence to:
J. J. Stryker,
jstryker@uvm.edu

Citation:
Stryker, J., B. Wemple, and A. Bomblies (2017), Modeling sediment mobilization using a distributed hydrological model coupled with a bank stability model, *Water Resour. Res.*, *53*, 2051–2073, doi:10.1002/2016WR019143.

Received 29 APR 2016
Accepted 9 FEB 2017
Accepted article online 15 FEB 2017
Published online 13 MAR 2017

Abstract In addition to surface erosion, stream bank erosion and failure contributes significant sediment and sediment-bound nutrients to receiving waters during high flow events. However, distributed and mechanistic simulation of stream bank sediment contribution to sediment loads in a watershed has not been achieved. Here we present a full coupling of existing distributed watershed and bank stability models and apply the resulting model to the Mad River in central Vermont. We fully coupled the Bank Stability and Toe Erosion Model (BSTEM) with the Distributed Hydrology Soil Vegetation Model (DHSVM) to allow the simulation of stream bank erosion and potential failure in a spatially explicit environment. We demonstrate the model's ability to simulate the impacts of unstable streams on sediment mobilization and transport within a watershed and discuss the model's capability to simulate watershed sediment loading under climate change. The calibrated model simulates total suspended sediment loads and reproduces variability in suspended sediment concentrations at watershed and subbasin outlets. In addition, characteristics such as land use and road-to-stream ratio of subbasins are shown to impact the relative proportions of sediment mobilized by overland erosion, erosion of roads, and stream bank erosion and failure in the subbasins and watershed. This coupled model will advance mechanistic simulation of suspended sediment mobilization and transport from watersheds, which will be particularly valuable for investigating the potential impacts of climate and land use changes, as well as extreme events.

1. Introduction

The detrimental impacts of suspended sediments on global freshwater ecosystems are well known [*Waters*, 1995; *Wilber and Clarke*, 2001; *Berry et al*., 2003; *Bilotta and Brazier*, 2008; *Vörösmarty et al*., 2010]. Suspended sediments and nutrients are considered two of the leading causes of water quality impairment in United States lakes and reservoirs [*US EPA*, 2000, 2002] and more recently has been one of the focuses of developing new water quality standards and criteria [*US EPA*, 2015]. Similarly the European Environmental Agency (EEA) has acknowledged that nonpoint pollution contributing to eutrophication and contamination of aquatic resources is a major environmental concern [*European Environment Agency*, 1995; *Stanners et al*., 1995]. According to the US Environmental Protection Agency (US EPA), suspended sediment directly impacts water clarity, scour, sediment storage, and other aspects of water quality. Suspended sediment can also transport bound nutrients such as phosphorus from cultivated land, and other binding contaminants [*Nebel and Wright*, 1993; *Sharpley et al*., 1994, 1995, *US EPA*, 2000, 2002; *Søndergaard et al*., 2003]. Excessive phosphorus and nitrogen concentrations can lead to harmful algal blooms (HABs) making sediment-bound nutrients an additional water quality concern associated with sediment transport [*Schindler et al*., 2008; *Paerl et al*., 2011].

Actively eroding stream channels have been observed in many regions where postglacial alluvial sediments dominate and stream channels have more recently undergone human modifications. In such regions, a significant portion of the total suspended sediment load reaching stream and river outlets can result from bank erosion and failure [*Kronvang et al*., 1997a, 1997b; *Laubel et al*., 1999; *Sekely et al*., 2002; *Simon et al*., 2004; *Evans et al*., 2006]. *Sekely et al.* [2002] used topographic surveys and field data to estimate that stream bank slumping contributed between 31% and 44% of total annual suspended sediment load at the mouth of the Blue Earth River in Minnesota, which represented between 7% and 10% of the annual total phosphorus load. Using the erosion pin method, *Huang* [2012] estimated that 67% of the suspended sediment

loading in an urbanizing watershed in Missouri resulted from stream bank erosion. The results of a study that used a mixing model and uncertainty analysis, conducted on six watersheds of Cayuga Lake, New York, determined that bank erosion contributed between 8% and 76% of annual fine sediment loads [*Nagle et al*., 2007]. Contributions of sediment from stream banks were particularly high where widespread and actively eroding glaciolacustrine deposits were present along streams. Several studies in Vermont watersheds, such as those of *Langendoen et al*. [2012], *DeWolfe et al*. [2004], and *Morrissey et al*. [2011] have also indicated that stream bank erosion, scour, and mass failure can account for anywhere from 30 to 80% of total sediment loading into streams and lakes. These last studies focused on volumes of sediment lost to erosion and failure, as opposed stream bank contributions to suspended sediment loads.

Empirical studies have demonstrated the importance of channel bank erosion on watershed sediment fluxes. In order to better quantify sediment loads from bank erosion, it is helpful to understand the conditions that drive bank erosion and failure processes. Activities such as channel straightening, removal of riparian vegetation, and urban development have also been shown to increase stream bank erosion [*Simon and Rinaldi*, 2006]. Stream banks can also represent a source of legacy phosphorus [*Kleinman et al*., 2011], particularly when adjacent to agricultural areas with long histories of fertilizer use. Large precipitation events and flooding that cause bank erosion and collapse can thereby result in pulses of sediment and associated phosphorus into streams and larger water bodies. In many regions, precipitation is becoming more intense [*Karl et al*., 2009; *Guilbert et al*., 2015] and therefore the need to simulate the impacts of changing precipitation climatology on nutrient transport into receiving waters will be of great value in informing management and policy actions. Although the need to represent stream bank contributions to sediment and nutrient budgets at the watershed scale is recognized, thus far mechanistic representation of both bank erosion and geotechnical failure processes in watershed models has remained elusive. Here we present a coupled modeling framework that addresses the prior shortcomings.

A range of bank erosion and channel evolution models exist for simulating river banks and channels, but none allow for full coupling to perturbations in the watershed. The Bank Stability and Toe Erosion Model (BSTEM) is a predominant bank stability model that simulates erosion and geotechnical failure of stream banks at a specific location or segment of channel based on limit-equilibrium analysis [*Simon et al*., 2000, 2003, 2011]. Alternatively, the stages of channel evolution described by *Schumm et al*. [1984] and later modified by *Simon* [1989, 1995] are the basis of most existing channel evolution models. These changes in morphology are represented as changes in the width and bed elevation of channel segments, where disturbance is first seen in lower channel reaches and then move progressively upstream. Current channel evolution models include numerical models such as those developed by *Darby et al*. [1996], *Nagata et al*. [2000], *Wang et al*. [2010], and *Xiao et al*. [2016], as well as the Enhanced CCHE2D model [*Duan et al*., 2001]. The National Sedimentation Laboratory developed the Conservation Channel Evolution and Pollutant Transport System (CONCEPTS), which simulates the evolution of incised streams and has been used to assess long-term impacts of stream stabilization measures and reduction of sediment yields [*Langendoen et al*., 1999, 2000, *Langendoen*, 2000, 2001]. CONCEPTS includes unsteady, one-dimensional flow, sediment transport and bed adjustment, bank erosion and channel widening processes, as well as representation of in-stream hydraulic structures such as bridges and culverts. These models do not typically include watershed processes that influence spatially variable soil characteristics, the effects of vegetation, or variable flow conditions.

Existing watershed models are also limited in their representation of sediment mobilized from the landscape, as to date they mostly incorporate surface erosion due to overland flow and landslide processes, and some include representation of fluvial erosion of stream channels. Catchment scale models have largely included sediment mobilization by sheet and rill erosion processes, and some include gully erosion. *Merritt et al*. [2003] as well as *Aksoy and Kavvas* [2005] reviewed in detail the range of erosion and sediment transport models that include representation of erosion processes. These models include a variety of conceptual, empirical, and physics-based models of varying spatial scales that simulate the generation of sediment as well as the transport of sediment. Some also include representation of pollutant transport. However, few include physics-based representation of rainfall-runoff processes, land surface sediment mobilization, and an in-stream model, much less the inclusion of stream bank erosion as well as mass failure of banks. The SHETRAN model for instance is such a watershed model that includes surface and gully erosion, as well as fluvial in-stream erosion [*Ewen et al*., 2000; *Bathurst*, 2002]. SHETRAN has been used to examine the effects

of basin and land use characteristics on overall sediment yield [e.g., *Lukey et al*., 2000; *Bathurst et al*., 2005; *Birkinshaw and Bathurst*, 2006]. However, no simulation of geotechnical bank failure is included in that model. Models to estimate erosion, point location bank failure, and sediment transport exist, however, a mechanistic model that can simulate changing contribution of stream bank sediment from erosion as well as geotechnical failure processes to an overall watershed sediment and nutrient load under changing climatic conditions has not yet been published.

Mechanistic hydrologic models are well suited for investigating the nonlinear impacts of changing land use and climate conditions on flow and stream bank erosion. The alternatives—empirical and probabilistic models—may be limited in applicability because the magnitude of a disruption or change can fall outside of the range of previously observed events, and in nonlinear systems past observations may not be adequate for predicting future response. Hence, a mechanistic model has better capability to represent sediment mobilization processes resulting from flows that exceed previous observations. The impacts of bank erosion and failure are increasingly important because of the changing climate and land use, and the ensuing potential for more frequent and higher magnitude flooding events. Here we present a coupled model approach to enable the representation of an important sediment source from the landscape and allow for perturbations in the watershed to impact the processes mobilizing sediment from stream banks.

2. Model Description

To address the need for mechanistic models to represent stream bank erosion and failure under changing climate and hydrologic regimes, we coupled two existing models: the Distributed Hydrology Soil and Vegetation Model (DHSVM) [*Wigmosta et al*., 1994] and BSTEM [*Simon et al*., 2000, 2003, 2011]. DHSVM is a mechanistic model that simulates water and energy fluxes at subdaily time steps at the watershed scale. BSTEM is a bank stability model that simulates toe erosion rates and failure events along channel reaches. Both models are described in full detail in associated publications and an overview of sediment related equations is provided in supporting information (S1). Below is a brief introduction to the models and discussion of processes related to the model coupling. A schematic of the coupled model processes, inputs and outputs is shown in Figure 1. A considerable number of different outputs can be specified in this modeling approach. Some, such as the occurrence of bank failures and the amount of sediment resulting from failures or erosion in a specific channel segment, are a result of the execution of BSTEM. Others, such as the concentration of suspended sediment in a channel segment or at the outlet of the watershed are the result of the coupled BSTEM and DHSVM functions.

BSTEM is a product of continuing research and development at the U.S. Department of Agriculture, Agricultural Research Service, National Sedimentation Laboratory (NSL). We chose BSTEM (Version 5.4) due to its advanced representation of both hydraulic and geotechnical processes contributing to bank failure. BSTEM has been used to investigate the impacts of reduced erosion on sediment loading from stream banks and has been modified for iterative use to estimate volumes of sediment originating from stream reaches [*Simon et al*., 2011]. It has also been applied to simulate long-term lateral retreat of stream banks [*Midgley et al*., 2012]. BSTEM comprises two components: a toe erosion module that simulates undercutting of banks resulting from fluvial erosion as a function of excess shear stress and a bank stability module that calculates a Factor of Safety (*FoS*) based on force equilibrium analysis [*Simon et al*., 2000].

DHSVM is a physics-based model that simulates water and energy fluxes at the land surface using a spatially explicit representation of topography, vegetation and soil properties. The model enables the user to represent modifications to the land surface, such as deforestation and urbanization [*Wigmosta et al*., 1994; *Wigmosta and Lettenmaier*, 1999; *Wigmosta and Perkins*, 2001; *Cuo et al*., 2008; *Surfleet et al*., 2010]. Topography drives the downslope movement of water, both across the land surface and within the channel network. All of the grid cells are linked hydrologically through the surface and subsurface flow routing. With respect to sediment, current versions of DHSVM include representations of surface erosion, hillslope erosion, mass wasting in the form of landslides and redistribution of mass downslope, as well as erosion of road surfaces [*Doten et al*., 2006]. The model has been applied to simulate impacts of forest management practices on land surface processes [*Storck et al*., 1998; *Bowling and Lettenmaier*, 2001; *Wigmosta and Perkins*, 2001; *Waichler et al*., 2005], as well as to study the interactions between climate change and hydrology [*Leung and Wigmosta*, 1999; *Wigmosta and Leung*, 2001; *Cuo et al*., 2009].

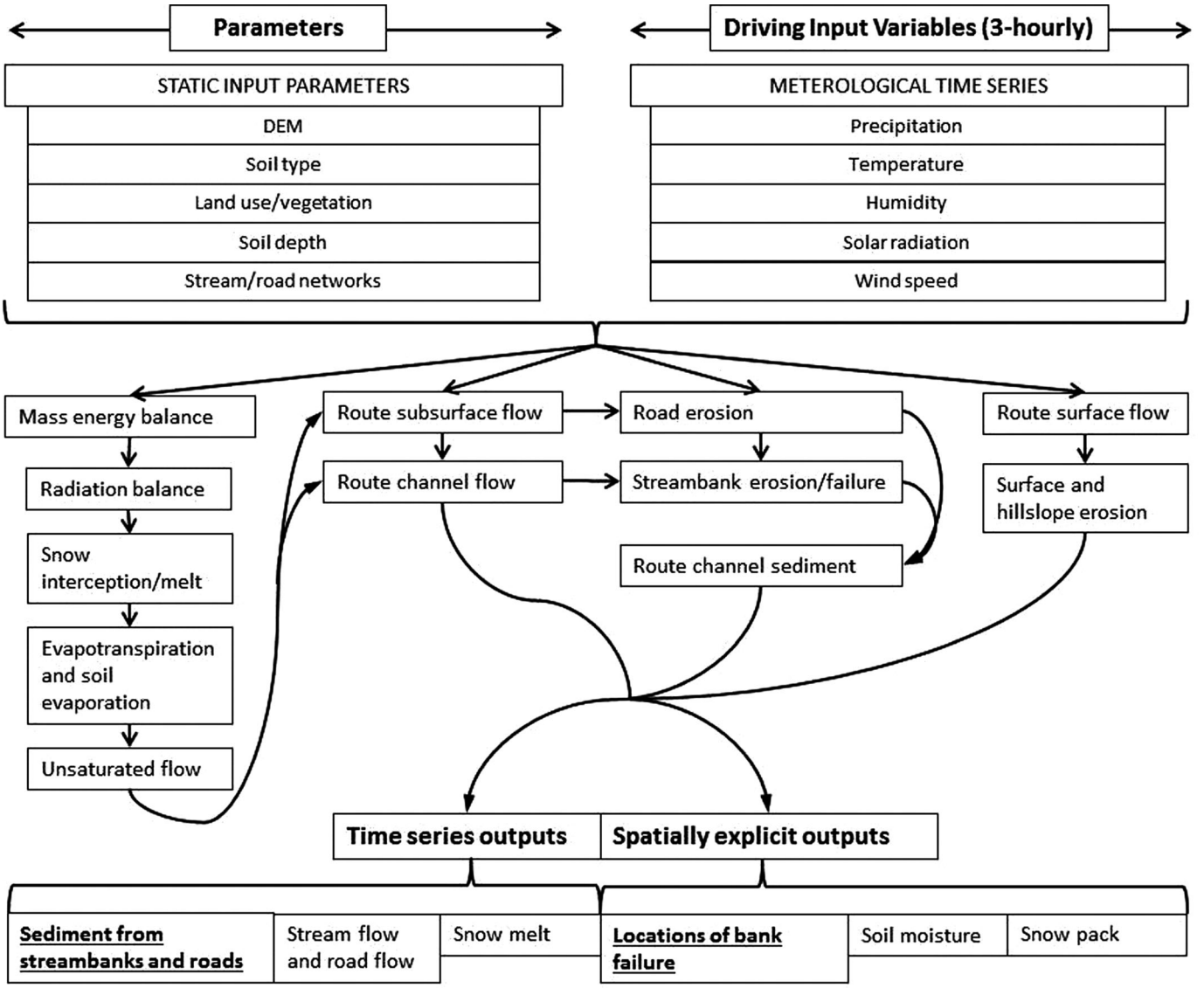

Figure 1. Schematic of coupled model processes, inputs and outputs. Although some outputs are the results of primarily the BSTEM algorithm (such as the occurrence of bank failures and the amount of sediment lost to bank erosion or failure in a specific channel segment), others are a result of the coupled functions of BSTEM-DHSVM (such as suspended sediment concentration in any stream segment or at the outlet of the watershed).

To improve the representation of sediment mobilization in DHSVM, we programmed the BSTEM algorithm, based on Version 5.4 as made available by the National Sedimentation Laboratory, into the DHSVM framework. The BSTEM algorithm is executed after channel routing is performed. At each grid cell in which a channel exists, the model first estimates toe erosion as described in the previous section, where flow depth and water table depth are the same as the water table in the corresponding DHSVM grid cell and based on discharge calculated in the flow routing functions of DHSVM. The bank profile updates if needed to represent changing geometry such as an actively undercutting bank (Figure 2). For each node on the bank profile that is below the stream water surface, the erosion distance (E) is calculated and the location of that node relocated accordingly (Figure 2). Once the effects of toe erosion have been implemented, the model executes a *FoS* analysis for each grid cell along the channel network. The *FoS* calculation is an instantaneous estimation of failure likelihood based on average conditions of the channel and bank material at that point in the simulation after erosion occurs. The algorithm loops over each node on the bank profile, randomly generating angles of potential failure planes and deciding on the most likely starting location for a failure plane. Next the model searches for

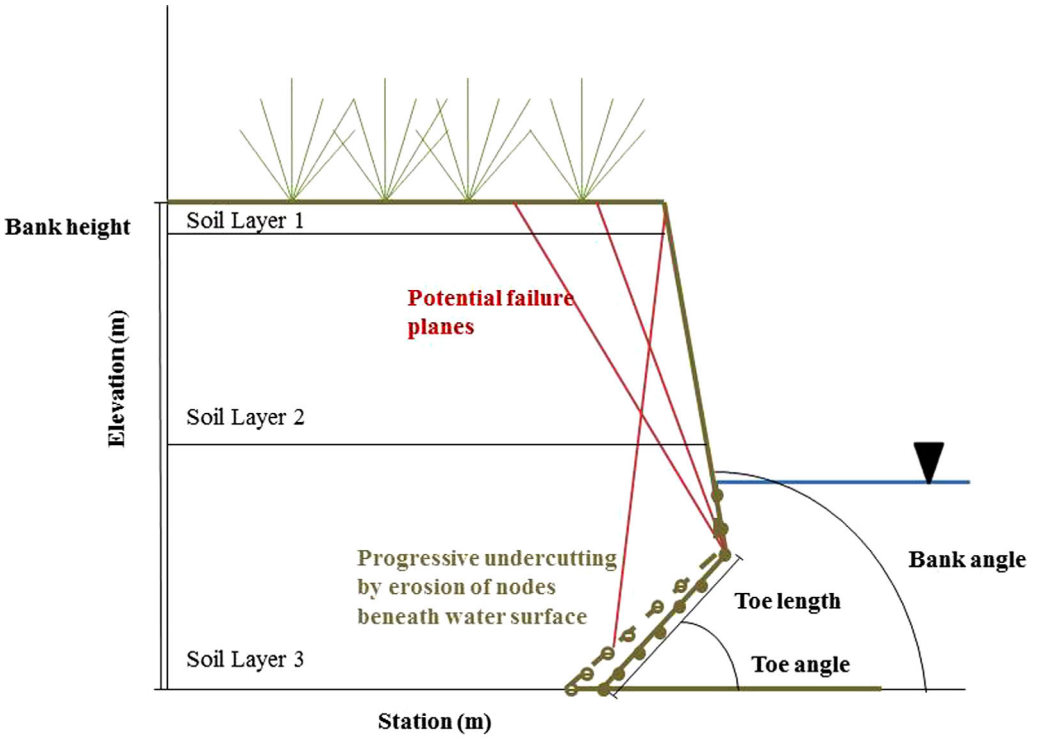

Figure 2. Representation of progressive undercutting and possible failures planes.

the most likely failure plane angle between calculated maximum and minimum angles, which are dependent on the minimum angle of the bank and the assigned friction angle of soil. The final *FoS* for that time step and grid cell with a stream bank is the *FoS* value of the most likely failure plane, based on searching through potential failure planes beginning at each node on the bank profile. If erosion or mass failure occurs in that grid cell, the mass of sediment is estimated for the portion of the channel within that grid cell and that sediment enters the stream network.

In the coupled model, sediment can thereby enter the stream network not only by overland and road erosion but also through bank erosion along a channel segment. Eroded and failed sediment combines with other local sediment inflows to the channel segment in the transport equation for total load as

$$\frac{\partial}{\partial t} m_s + \frac{\partial}{\partial x} ACV\rho_s = \rho_s (q_s + q_{sb}), \tag{1}$$

where q_{sb} is the local volumetric sediment inflow rate to the channel reach per meter length ($m^3/s/m$); q_s is the local volumetric sediment inflow rate to the channel reach per meter length ($m^3/s/m$); ρ_s is particle density of the sediment (kg/m^3); m_s is the mass of stored sediment in the bed per meter of channel length (kg/m); A is the cross-sectional flow area (m^2); C is the total sediment concentration (m^3/m^3); and V is the average channel flow velocity (m/s). This sediment is then transported throughout the channel network and potentially to the watershed outlet based on the existing DHSVM routing functions (further described in supporting information (S1)).

As sediment is routed downstream through the channel network [*Doten et al.*, 2006], the coupled model tracks the proportion of sediment originating from stream banks (Figure 3). For each channel segment, the ratio of stream bank inputs to all other sediment inputs is calculated as

$$R_m^i = \frac{((R_{m-1}^i * U_m^i) + (R_m^{i-1} * \Delta SS_m^{i-1}) + B_m^i)}{(U_m^i + \Delta SS_m^{i-1} + B_m^i + Or_m^i + Ol_m^i + D_m^i)}, \tag{2}$$

where m is the channel segment identifier, i is the time step, B is sediment from stream bank erosion/failure, Ol is sediment from overland inflow, Or is from over road inflow, D is debris inflow, U is inflow from

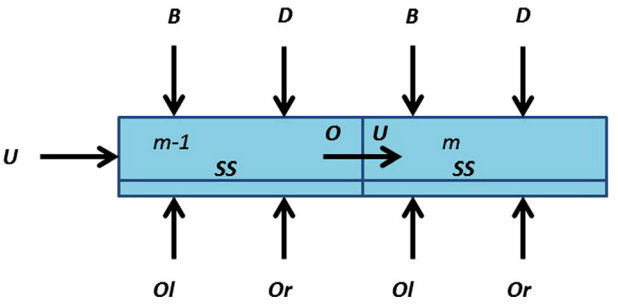

Figure 3. Representation of inputs to each channel segments m and $m-1$, where m is the channel segment identifier, B is sediment from stream bank erosion/failure, Ol is sediment from overland inflow, Or is from over road inflow, D is debris inflow, O is outflow from the upstream segment, U is inflow from upstream segment, and SS is stored sediment in that channel segment.

upstream segment, and ΔSS is the change in stored sediment between the previous and current time step. This results in an estimate of what percentage of total sediment at the watershed outlet, or at any chosen location, originated from stream bank erosion and failure.

DHSVM input files include a configuration file to assign soil and vegetation parameters based on raster maps of soil and land use types which are prepared using ArcGIS. Where possible, the BSTEM module uses the same parameters as those required by other DHSVM functions (Table 1). For example, soil layers in BSTEM are defined based on the same soil depths set in the DHSVM input file as are certain properties of those soil layers such as porosity. Information calculated dynamically in DHSVM also provides input data for BSTEM. For example, the BSTEM algorithm activates after subsurface conditions and flow routing are calculated, so water table and flow depth at each time step and in each grid cell are used to inform BSTEM of within-bank water table level and channel flow surface levels, respectively. We modified the configuration files to include additional parameters needed for BSTEM calculations, which were set either by soil, vegetation, or stream class. We also assigned additional physical attributes of the channels (including bank and toe angle, bank height, and bank toe length) based on the channel classes as set in the DHSVM channel network input files. In the case of soil cohesion and friction angle of the soil (which influence both surface erosion from the landscape and BSTEM calculations), DHSVM assigns these parameters to soil types. However, since these parameters were different for stream bank soils than for soils further away from streams, these two parameters were separately assigned to bank soils based on channel class. Radius of curvature was also assigned based on channel class. Specific inputs to the model are described in later sections.

3. Model Test Application

3.1. Study Area

For initial assessment of our approach, we modeled the Mad River watershed (Figure 4) in central Vermont, a tributary of the Winooski River. The watershed drains approximately 373 km^2 and ultimately empties into Lake Champlain, which itself is part of the St. Lawrence basin. The steep valley is bordered by the Green Mountains, which are composed of highly metamorphosed rock with widespread glacial deposits along the valley floors [*Field Geology Services*, 2007]. Elevation ranges from approximately 70 to just over 1200 m. A mix of surficial geologic deposits exist in the watershed, including glacial tills in the highlands, glaciofluvial deposits along the valley margins, and alluvial fan deposits near tributary and main stem junctions [*Whalen*, 1998; *Dunn et al*., 2007a, 2007b]. In the lower reaches, erodible glaciolacustrine deposits commonly underlie alluvial deposits, which contribute to the sensitivity of both major tributaries and the main stem of the Mad River to changes in land use [*Barg and Blazewicz*, 2003; *Dunn et al*., 2007a, 2007b; *Nagle et al*., 2007].

Table 1. Shared and Added Parameters, Relevant to the Addition of BSTEM to DHSVM, As Well As Parameters That Were Similar in the Two Models But Also Assigned in the Coupled Model Based On Channel Class for Bank Soils

Shared Variables and Parameters	Added BSTEM Parameters	Similar, Reassigned Parameters
Flow depth (m)	Bank angle (°)	Soil cohesion (kPa)
Water table depth (m)	Bank toe angle (°)	Friction angle (°)
Channel segment width (m)	Bank toe length (m)	Saturated unit weight (kN/m^3)
Channel segment length (m)	Critical shear stress of bank material (kPa)	
Bank height (m)	Critical shear stress of toe material (kPa)	
Manning's n of channel	Particle diameter, d_{50} (mm)	
Soil depth (m)	Internal friction angle (°)	
Soil layer thicknesses (m)	Angle due to matric suction (°)	
	Radius of curvature (m)	

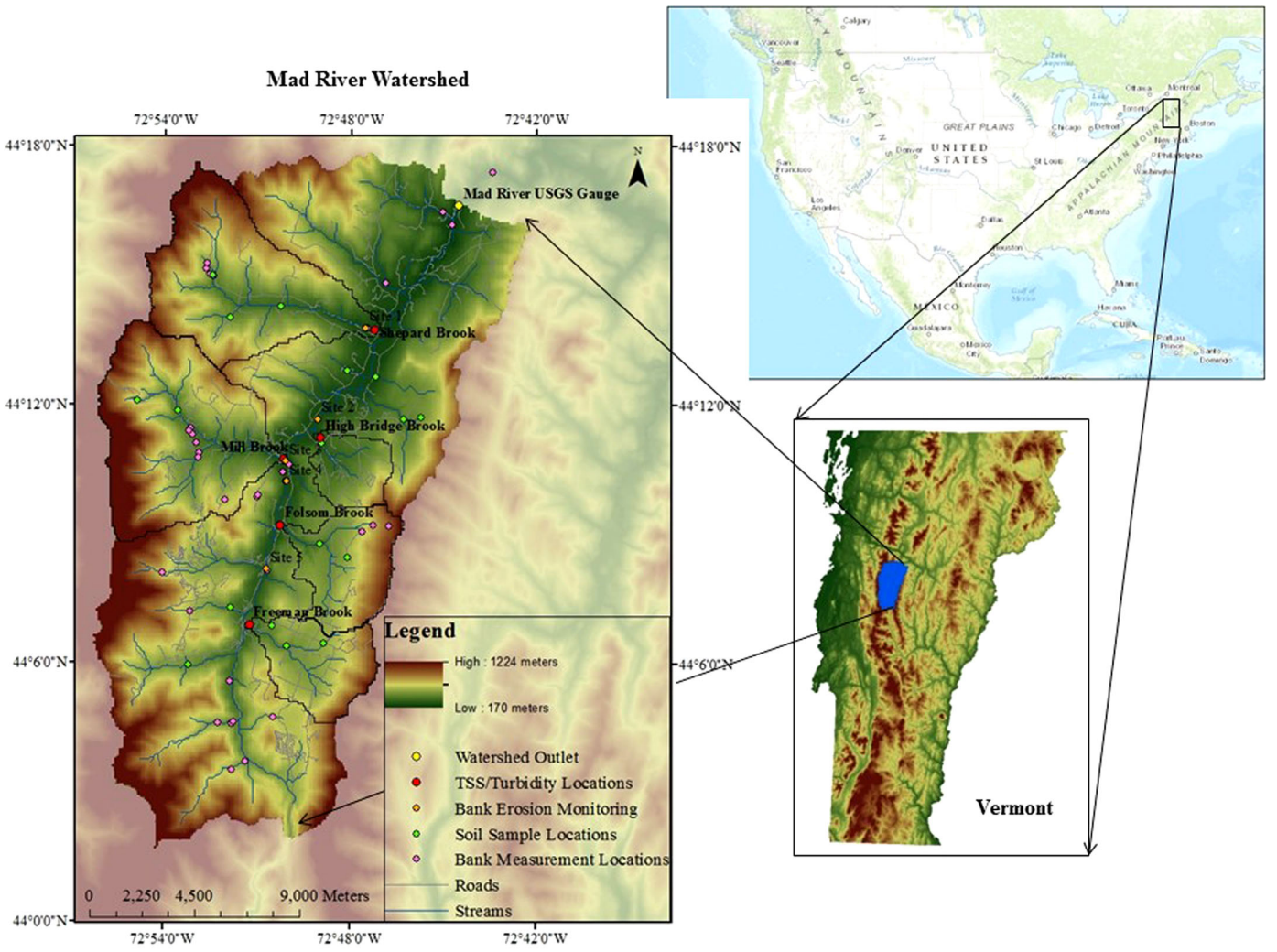

Figure 4. Mad River watershed, Vermont. Map shows the five subbasins included in this study, locations of bank monitoring sites (BST), bank profile measurements, additional soil samples locations (bulk density and grain size analysis), and TSS/turbidity measurements.

Following European settlement, the watershed experienced a period of deforestation and mill dam construction in the nineteenth century and early twentieth, followed by a period of forest regrowth [*Foster and Aber*, 2004; *Field Geology Services*, 2007; *Kline and Cahoon*, 2010]. Although mill dams existed in the watershed and have largely been removed, local geomorphology is more strongly influenced by postglacial deposits and legacy sediments from deforestation, as well as from significant climate events and changes [*Whalen*, 1998; *Dunn et al*., 2007a, 2007b; *Walter and Merritts*, 2008]. More recently, the area has become a popular destination for vacationers. Additional development has occurred in the form of homes, ski resort facilities, and associated commercial areas.

Human alterations, as well as the geologic setting and occurrence of natural incision processes, have influenced the channel morphology and hydrology of the watershed, making it susceptible to the impacts of floods and extreme precipitation events. Channel incision exacerbates the sediment and phosphorus transport problem by naturally impairing stream channels, translating flood waves downstream instead of dissipating the energy contained in high flows. Bank erosion is therefore an issue of concern in the Mad River watershed, and has been documented in a series of Geomorphic Assessments issued by the Vermont Agency of Natural Resources [*Field Geology Services,* 2008; *Fitzgerald and Godfrey,* 2008; *Parker et al.,* 2008]. Concern over erosion and failure of stream banks arises due to reasons discussed previously. Particularly along the main stem and main tributaries of the Mad River, undercutting and erosion of banks can be visibly observed. Figure 5 shows an example of

Figure 5. Photo of undercut and eroding bank along Mad River main stem channel, near Lareau Farm Inn in Waitsfield, VT (Site 4 in Figure 5).

undercutting along a section of the Mad River main stem, near the town of Waitsfield in the center of the watershed.

A USGS gaging station is located near the outlet of the Mad River watershed in Moretown, Vermont (#04288000) and has been collecting data since 1927. Based on data downloaded from this station, average annual flow (for USGS water years, which extend from October through September) from 1929 through 2015 was 7.7 m^3/s, and ranged from 3.8 to 13.8 m^3/s. Peak annual streamflow ranged from 35 to 685 m^3/s between the years 1927 and 2015, with the flood of record occurring in August 2011 during Tropical Storm Irene. The 2 year return flow is approximately 169 m^3/s based on those 86 years of annual flow data (approximately 608,400 m^3/h for comparison to subsequent flow plots).

Five tributaries were included in this study: Mill Brook, Shepard Brook, Freeman Brook, Folsom Brook, and High Bridge Brook (Figure 4). These subbasins represented a range of land use types and elevations that are found in the Mad River watershed. Table 2 presents relevant characteristics of these subbasins, including area, road-to-stream length ratio, and percent coverage of potentially influential land cover types. These subbasins were selected to make use of previous studies [*Wemple*, 2013; *Hamshaw*, 2014], described below, for model validation.

3.2. Meteorological Data

Climate variables—primarily precipitation—drive the hydrological processes that can cause stream bank erosion and collapse. DHSVM requires several input variables at a relatively high temporal resolution: precipitation, temperature, humidity, incoming short wave radiation, incoming long wave radiation, and wind speed. We installed a meteorological station for the purpose of acquiring local high resolution data near the center of the watershed at an elevation of approximately 208 m asl. This station began recording 31 July 2013.

Table 2. Proportional Characteristics of Subbasins Including Road-to-Stream Length Ratio and Land Cover Proportions

	Mad River Watershed	Mill Brook Subbasin	Shepard Brook Subbasin	Freeman Brook Subbasin	Folsom Brook Subbasin	High Bridge Subbasin
Total area, km^2 (percentage of watershed)	359.0 (100%)	49.3 (13.7%)	44.8 (12.5%)	16.6 (4.6%)	18.5 (5.2%)	9.1 (2.5%)
Road:stream length ratio	1.9	1.8	1.2	15.1	1.6	3.6
Percent agriculture and pasture (%)	4.4	3.8	2.8	15.4	14.7	22.6
Percent urban/residential (%)	5.5	2.9	10.0	4.0	1.9	5.6
Percent roads/transportation (%)	2.1	3.4	2.5	4.5	2.9	7.6
Percent forest (conifer, deciduous, mixed) (%)	86.5	85.4	91.3	73.5	78.8	62.0

In addition to the meteorological station data, we used National Centers for Environmental Protection (NCEP) reanalysis data provided by the NOAA/OAR/ESRL PSD, Boulder, Colorado, USA (http://www.esrl.noaa.gov/psd/). The North American Regional Reanalysis (NARR) data are generated using the high resolution NCEP Eta Model, with a grid resolution of 32 km, along with the Regional Data Assimilation System (RDAS). The resulting product is a high resolution combined model and assimilated time series data set and was available at a 3 h temporal resolution. We obtained this data for water years 2009–2014. In August 2011, Tropical Storm Irene passed through Vermont, resulting in storm total precipitation of 7.5–12.5 cm across the region. NARR data did not reflect the magnitude of this event in the grid cells covering the Mad River watershed, as measured by Doppler radar. Since one of the primary objectives of this coupled approach is to represent impacts of extreme events, such as what occurred as a result of Irene, we used local spotter reports of storm totals to replace NARR Reanalysis precipitation for the Irene event [*National Weather Service*, 2011]. The distribution of rain over the storm period was kept the same as seen in NARR data, but increased in magnitude to equal locally observed rainfall totals over the storm period.

Although only a limited time period of measured data was available, these data were used to drive the model for examining the representation of sediment in the coupled model application. Differences between NARR and measured data were clear, and were attributed to the coarse resolution of the NARR product as well as the inability of that product to predict local convective storms that occur during the summer months. A full comparison of NARR and measured variables in included in supporting information (S2.1). NARR data were therefore used only to validate the hydrological calibration over several additional years.

3.3. Inputs and Field Data

DHSVM requires GIS-derived inputs, as well as configuration files containing user-defined parameter values. Wherever possible we used site specific data collected in the field to inform parameter values, and remaining values were assigned based on literature-cited values. We generated topography layers using USGS National Elevation Dataset (NED) 10 m data, aggregating this to a resolution of 100 m (m) for the entire Mad River watershed. We classified soil based on Natural Resources Conservation Service (NRCS) hydrologic soil units and land use based on the 2006 National Land Use Cover Dataset (NLCD). We generated soil depth layers as a function of elevation data and minimum/maximum soil depths, using scripts that accompanied the DHSVM source code downloaded from the University of Washington Land Surface Hydrology Research Group website (http://www.hydro.washington.edu/Lettenmaier/Models/DHSVM/).

To inform parameter values, we collected additional field data on channel and soil characteristics. In this work, road classes and characteristics were based on road surface characteristics provided by the Vermont 911 board and obtained from the Vermont Center for Geographic Information. The stream channel network was delineated using ArcGIS and stream classes were assigned based on contributing drainage area. These channel classes are the basis for parameter assignment described in subsequent sections. Parameters describing the bank profile are also set by stream class. In addition, to calculate the volume of sediment mobilized from a stream bank, the erosion rate calculated for any segment is currently applied to half the length of the channel segment present in that cell. Similarly, if a failure occurs, it occurs along half the length of the segment in that cell. Because we used a 100 m resolution, and a relatively coarse stream delineation, the application of the erosion rate or failure to the entire length of the channel was expected to overestimate the volume of sediment originating from stream banks. We chose half the channel length based on *Morrissey et al*. [2011], in which authors indicated that stream bank erosion affected 47–72% of reach lengths.

BSTEM requires the user input bank geometry either as a series of 23 points that describe the detailed geometry of the bank, or as several measurements that are used to compute a simplified geometry (BSTEM v5.4). For this work, we programmed the second option into DHSVM, so that the user inputs bank height, bank angle, toe length, and toe angle (Figure 2) for each channel class in the stream input file. Based on these parameters, BSTEM calculates a simplified bank profile. We made 35 measurements across all stream channel classes of these parameters describing the stream bank profiles (pink circles in Figure 4); we used these data to set initial bank profiles for each channel class. As the model progresses and bank erosion or failures occur, the bank angle, toe length, and toe angle can evolve during simulation. The elevation of the bank height remains constant as the flood plain elevation; however, individual nodes along the bank profile can decrease in elevation due to failure and erosion. In order to prevent instabilities in the model, the bank profiles are reset at the beginning of the water year. (If allowed to retreat over multiple years without being

reset, the x and y positions of banks can become large negative numbers.) However, the mass of progressive erosion and failures are continuously stored and not reset. Other details on stream inputs are included in supporting information (S2.2).

Local field data collected between 2012 and 2015 provided information used to set model parameters, as well as to calibrate and validate model results. Field work included erosion monitoring at specific sites, measurements of bank profiles throughout the watershed, soil testing and investigation of bank parameters, as well as grab samples for analysis of total suspended sediments (TSS). Several sites were chosen for bank erosion monitoring and further investigation of geotechnical soil properties (yellow circles in Figure 4); these sites were located mostly along the main stem of the Mad River and were chosen based on observed and anticipated bank activity, site vegetation and physical characteristics, as well as accessibility. Bank soils at these sites were largely composed of silt loam and sandy loam and considered representative of soils along the main stem and major tributaries. Vegetation along the main stem of the Mad River was dominated by the invasive Japanese knotweed (*Fallopia japonica*), however, sites were chosen to include some variation in vegetation as well. Other vegetation observed at monitored sites included pasture grasses, forested areas, and native perennial species such as Canadian goldenrod (*Solidago canadensis*). We also collected soil samples at 20 locations in the watershed (green circles in Figure 4) for grain size and bulk density analysis. Additional information regarding field data is included in supporting information (S2.2).

The BSTEM algorithm requires the definition of parameters related to geotechnical properties of soil and additional stability provided by roots or bank protection measures. Critical shear stress and erodibility parameters were set initially based on previously described measurements taken by *Hanson* [1990], *Hanson and Simon* [2001], and *Simon et al.* [2003] using an in situ jet-test device. We conducted borehole shear testing (BST) at the identified stream bank monitoring sites (Figure 4) to obtain in situ measurements of soil cohesion and friction angle. Most monitored sites comprised relatively similar sandy soils with an underlying gravel layer and results from the bore BSTs indicated little difference in cohesion and friction angle between sites (supporting information Table S1). We assigned cohesion and internal friction angle to bank soils in each grid cell (that contained a stream channel) based on user-defined probability distributions in order to account for normal spatial variability in these parameters. We also explicitly assigned radius of curvature and added cohesion values to each stream segment using probability distributions defined by field-based data. Radius of curvature represents sinuosity, and added cohesion represents the influence of vegetation or bank stability measures to each stream segment. Separate probability distributions were defined for each channel class and values were assigned to each grid cell containing a bank segment during initialization, then held constant for the duration of the model run. Thereby a stream segment randomly assigned a high curvature value would see more progressive undercutting than a straighter stream segment over longer time periods. The parameters assigned probabilistically therefore also remain constant during execution of the BSTEM algorithm in each grid cell.

We also used suspended sediment data presented by *Hamshaw* [2014] collected at the outlet of the Mad River near Moretown, as well as at the outlets of the five previously mentioned tributaries. Based on high temporal resolution turbidity monitoring and measurements of suspended sediment, Hamshaw developed TSS-turbidity relationships to assist in training an artificial neural network (ANN) for the Mad River watershed. He estimated suspended sediment loads based on the theoretical equation

$$Load = \int_{t_1}^{t_2} Q_t TSS_t dt, \tag{3}$$

where Q_t is the stream discharge at time t and TSS_t is the total suspended sediment concentration at time t. Loads were calculated using turbidity-based estimates of TSS and compared to loads calculated using estimates of TSS based on the traditional sediment rating curve approach (SRC). In this study, we used Hamshaw's continuous turbidity-based estimates of TSS to calculate suspended sediment load at the outlet for the period of 1 August 2013 to 30 November 2013 and for 15 June 2014 to 31 October 2014 for comparison to modeled loads. We also used discrete sample results taken during these time periods to assess modeled suspended sediment at the watershed and subbasin outlets (red circles in Figure 4).

3.4. Calibration and Validation Methods

To assess the functionality of this coupled modeling approach, we focused first on flow and then results of simulated sediment mobilization in the watershed. We used measured meteorological data from the field

station, for the 2014 water year (1 October 2013 to 1 October 2014), to achieve initial hydrological calibration and compared model flow results to flow data from the USGS gauge at Moretown, Vermont. Although DHSVM has a relatively large number of input parameters, previous studies have indicated that the model is mostly sensitive to a few key parameters [*Wigmosta et al*., 2002; *Yao and Yang*, 2009; *Surfleet et al*., 2010; *Cuo et al*., 2011]. Based on these previous studies, we chose lateral conductivity, a factor representing exponential decrease in conductivity with depth, field capacity, and porosity as calibration parameters and we manually modified these within realistic ranges to adjust stream flow. We then ran the model with the same parameter set for several years using NARR data to validate model performance. The model spin-up period was 1 year for all model runs and was driven by NARR data.

Several measures of fit were chosen to assess model performance with respect to flow. For the initial calibration period, driven by measured meteorological data, we primarily used the Nash-Sutcliffe efficiency [*Nash and Sutcliffe*, 1970] (E_2). E_2 is a commonly used measure of fit for hydrological models and ranges from $-\infty$ to 1.0, where 1.0 indicates a perfect fit and 0.0 indicates the model results are no better than the mean value of the observed data set. We further assessed model fit for these multiyear model runs using two additional measures proposed by *Legates and McCabe* [1999] and described by *Waichler et al*. [2005] to incorporate inherent seasonal variability in flow data. These additional measures included the baseline-adjusted first-degree efficiency (E_1'), where the baseline mean was defined as the mean for each month of the year, taken across all years in the simulation period, as well as the baseline-adjusted modified index of agreement (d_1') [*Waichler et al*., 2005]. E_1' has a range of $-\infty$ to 1.0 and d_1' ranges from 0 to 1.0. These additional measures of fit are of particular interest in assessing multiyear simulations but were also calculated for initial runs done with locally measured meteorological data for consistency.

Following calibration/validation of model hydrology, we calibrated sediment generation in the watershed using TSS data from four locations in the watershed. All sediment results presented here were generated using measured meteorological data since this produced better hydrology results and better represented actual conditions in the watershed. Additionally, subsequent results are the average of 10 identically parameterized runs. This was to account for probabilistic variation in explicit parameter definition as well as in failure calculations. Again, we used average bank d_{50} and critical shear stress values as the primary calibration parameters for the stream bank sediment module.

We used three independent data sets to assess the ability of our coupled model to estimate sediment fluxes. Data from *Hamshaw* [2014], who used high frequency turbidity sensing and discrete TSS sampling on our five study subbasins to establish high temporal resolution estimates of TSS concentrations and suspended sediment flux, were used to evaluate model performance and as validation of our estimates of basin-scale sediment flux. We compared modeled suspended sediment loads for the Mad River watershed to those estimated using continuous turbidity-based TSS [*Hamshaw*, 2014], for the nonwinter months of 2013 and 2014. We also used 2013–2014 discrete TSS measurements [*Hamshaw*, 2014] at four locations in the watershed (red circles in Figure 4) to examine model performance at discrete times and locations. The locations included the outlet of the Mad River at Moretown and the outlets of three of the subbasins, Mill Brook, Shepard Brook, and Folsom Brook. Too few samples taken at Freeman Brook and High Bridge subbasins coincided with modeled periods, so these were not used for discrete sample comparison. For these four locations, radius of curvature values was hardcoded into model initialization functions, instead of assigned based on the stream class probability distribution. In addition, data from *Wemple* [2013], who used storm-based sampling of road-sediment fluxes and a simple GIS-based model for basin-scale estimates, were compared to modeled results of road-generated sediment flux.

Although we have no field data on the relative contributions of overland flow or stream bank erosion, we lastly examined the proportions of simulated sediment mobilized throughout the watershed by overland erosion, road erosion, and stream bank erosion or failure. We also looked at the proportions of sediment from each of these mechanisms at the outlet of the Mad River at Moretown and the outlets of all five subbasins (which is not necessarily the same and the amount mobilized due to settling of larger sediment). The goal of this last investigation was to assess whether the relative proportions of sediment changed and whether characteristics of the subbasins, had an impact on simulated sediment.

4. Results of Coupled Model Application

4.1. Flow

Based on visual comparison as well as measure of fit values, the simulated watershed discharge fit well in the runs driven with measured meteorological data ($E_2 = 0.76$, $E_1' = 0.47$, $d_1' = 0.73$) and was considered adequate for runs driven with NARR data ($E_2 = 0.67$, $E_1' = 0.32$, $d_1' = 0.67$) for all 4 years). The model performed very well for the 2011 and 2012 water years ($E_2 = 0.90$ and 0.92, $E_1' = 0.50$ and 0.52, $d_1' = 0.92$ and 0.94, respectively); however, results for 2013 and 2014 water years did not show such a good fit (Figure 6). Figure 6c shows that the model did not simulate several discharge peaks, particularly during the summer months of 2013. We expect that these events were driven by local convective storms and that NARR data did not represent small scale weather events such as these local storms. The largest discrepancy in 2014 was the spring melt period. Small changes in temperature can drive these melt processes and NARR temperatures likely did not accurately reflect those small fluctuations in temperatures that impacted snow melt throughout the watershed. This again is likely a result of the NARR data resolution and the ability of that data to represent local weather patterns and the effects on local hydrological processes.

4.2. Sediment

We first examined simulated sediment mobilization with respect to flow and watershed conditions. Figure 7 shows the model discharge at the watershed outlet and total sediment mobilized in the watershed during

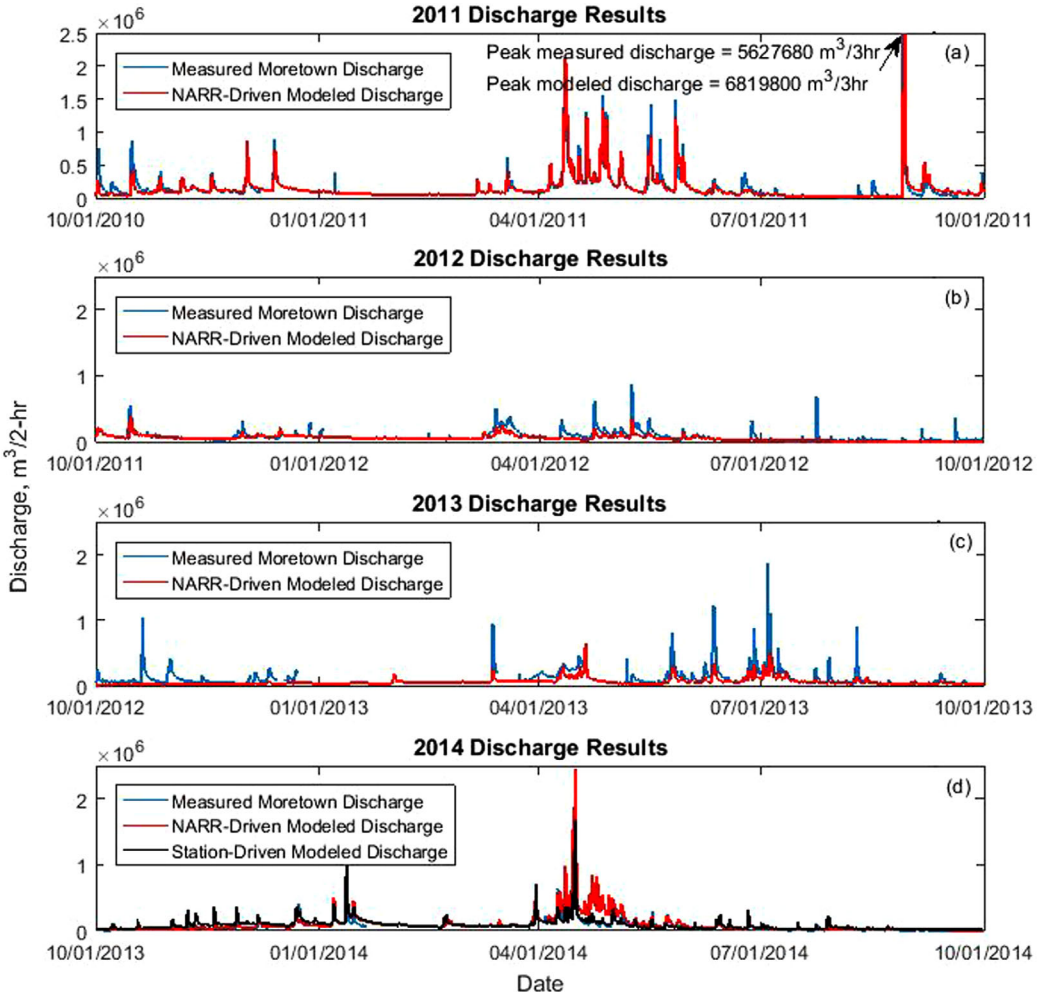

Figure 6. Measured verses modeled flow data for water years 2011–2014. The 2011–2013 runs were driven by NARR data and for the 2014 water year, runs were conducted using both measured station data and NARR data. These plots reflect gaps in the measured USGS data, where the gauge was unable to record, mostly due to winter ice conditions.

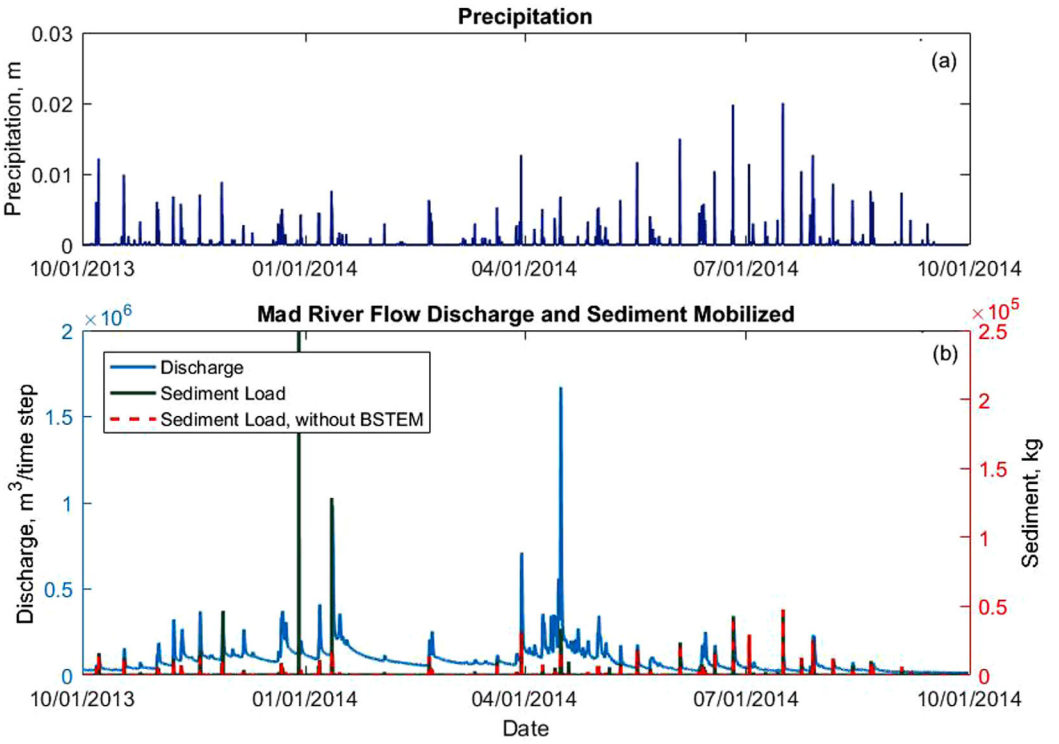

Figure 7. (a) Measured precipitation (model input) and (b) model simulated discharge at the Mad River outlet and total simulated sediment mobilized within watershed (b).

the 2014 water year (Figure 7b), as well as precipitation during that time period (Figure 7a). Sediment mobilization generally corresponds with peaks in flow, although as expected, the amount of sediment mobilized is not linearly related to the peak in discharge. The sediment pulses seen in Figure 7b are the result of bank failures. Failures that occurred in January 2014 corresponded with temperatures above freezing, indicating a midwinter thaw, as well as the occurrence of precipitation. Relatively few failures were seen during the period of high flows resulting from snow melt, likely because no significant precipitation events occurred during that time period. Erosion and failure of stream banks is affected by not only high flows but also the intensity and persistence of precipitation, as well as antecedent conditions such as soil moisture and vegetation. Smaller amounts of sediment enter channels at lower flow events; this sediment is the result of erosion processes (as opposed to mass failures), from stream banks, as well as overland and road erosion. It should be noted that Figure 7b shows total mobilized sediment entering stream channels, and not sediment output from the watershed. A portion of suspended sediment is deposited before reaching the outlet.

We compared model predicted suspended sediment concentrations to discrete suspended sediment measurements taken during summer months of 2013 and 2014 at the Mad River outlet and three subbasins (Figure 8). Not enough samples were taken within the modeled time period at Freeman Brook and High Bridge Brook to compare with model results. Although the inclusion of BSTEM does not change suspended sediment concentrations for all events, it does improve the representation of high concentrations associated with higher flow events as well as produce peaks during some small events that otherwise were not present (Figure 8d). For example, in the subwatersheds, the inclusion of BSTEM had the most impact on suspended sediment concentrations during spring melt (shown in Figure 8b), however, no samples were taken during that period. The model simulates relatively well the occurrence of sediment peaks, and in most cases the magnitude of those peaks are comparable. The model generally underpredicts suspended sediment concentration in comparison to samples, particularly at the subbasin outlets. We attribute this to the rapid response of subbasin discharge during flow events and the temporal resolution of the model being too coarse to capture those fluctuations. In many cases, there were multiple TSS samples that showed considerable variation and were taken within a single model time step (2 h).

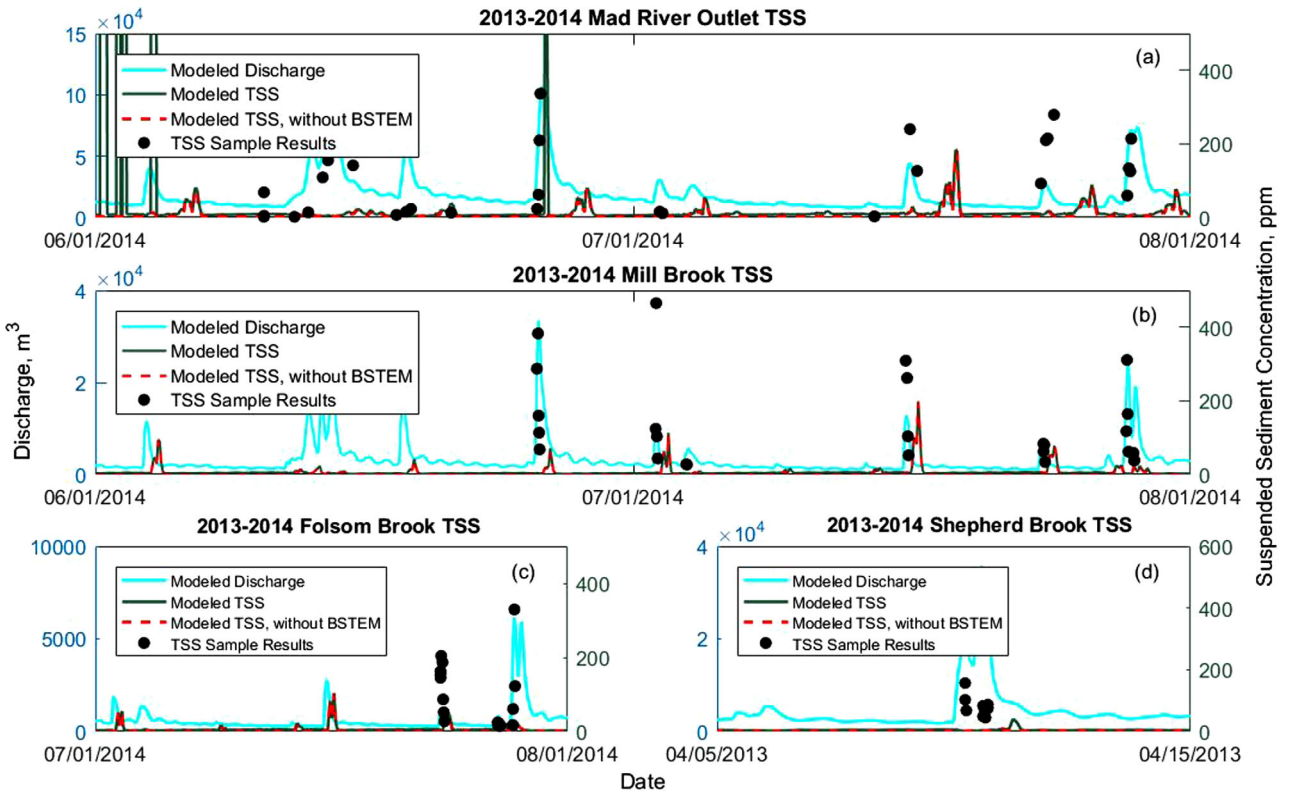

Figure 8. Suspended sediment concentrations at the Mad River and subbasin outlets. (a, b) Suspended sediment for the period 1 April 2014 through 31 August 2014 at the Mad River and Mill Brook outlets. (c, d) Results for a single storm event at Shepard and Folsom Brook outlets. Figure 8 also indicates sediment results produced when the model is run with the same parameter set but the BSTEM module inactivated.

For most events, Figure 8 shows a lag in modeled sediment, particularly at the outlet of the larger watershed (Figure 8a). Few studies have compared DHSVM-modeled sediment concentrations to site specific suspended sediment measurements such as this, though two works have noted similar lags in sediment ranging from −9.5 to 26.5 h and from 1 to 37 h behind discharge peaks [*Beeler*, 2014; *Clement*, 2014]. *Clement* [2014] suggested that variability in lag times between turbidity and discharge were related to precipitation pattern, where longer lag times were associated with higher duration, lower intensity events and could indicate the occurrence of a mass failure event. In this application lag times at the watershed outlet were approximately 60 h (30 time steps), while at the major tributary outlets (Mill Brook, Shepard Brook, Folsom Brook, and High Bridge Brook) the lag time ranged from 8 to 14 h (4–7 time steps). At the outlet of Folsom Brook sediment typically lagged only 2 h (1 time step) behind peak discharge. No discernable pattern of lags was found in the modeled versus measured discharge; peak modeled discharge occurred almost simultaneously with measured peak discharge (±2 h/1 time step). We believe the lag observed in modeled suspended sediment is related to the temporal and spatial resolution of the model and the number of model steps required to move sediment from various locations in the watershed to the channel network and then downstream to an outlet segment. In the current model, sediment supply is not limiting, but transport may be limited by estimation of flow conditions over the 2 h time step. Pulses of sediment from simulated bank failures can be seen immediately following peak discharge in some cases (Figure 8a). These likely occurred within close proximity to the outlet, resulting in less lag time (2–4 h, 1–2 time steps) than occurred with sediment originating further from outlet points, such as from upland erosion of land or road surfaces or upstream erosion of banks.

We compared cumulative total load, calculated using *Hamshaw*'s [2014] turbidity-based TSS data, to cumulative modeled load at the watershed outlet (Figure 9). Modeled load is similar to the field-estimated load for the nonwinter months of 2013, although again underestimates loading in 2014. The modeled cumulative sediment load for 1 August 2013 to 25 November 2013 was approximately 1,240,000 kg, which was lower than the 1,960,000 kg estimated using data from the work of *Hamshaw* [2014]. However, the modeled

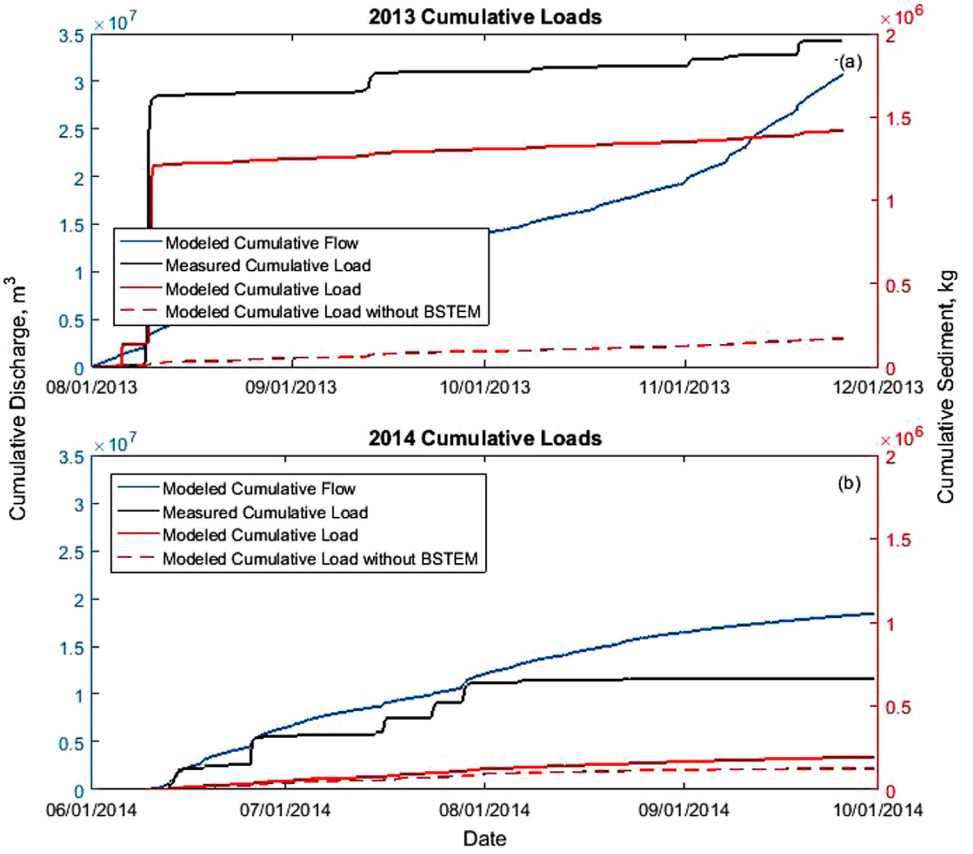

Figure 9. Modeled verses measured cumulative sediment load at outlet of Mad River watershed during modeled nonwinter months in 2013 and 2014. Measured sediment load was based on turbidity-estimated TSS [*Hamshaw*, 2014].

cumulative load with BSTEM inactivated was approximately 667,000 kg for the same period. For 6 June 2014 through 5 December 2014, modeled cumulative load was approximately 345,000 kg and estimated load was 666,000 kg, where the modeled load with BSTEM inactivated was approximately 125,000 kg. The model underestimates suspended sediment loads in comparison to the field-based estimates of loading at the watershed outlet. In particular, the simulated peaks in suspended sediment due to specific precipitation and high flow events are underpredicted while there is some overprediction of suspended sediment concentrations during base flow conditions. While calibrating this model, we observed a trade-off between simulating elevated base flow suspended sediment as well as increased numbers of failures and simulating base flow accurately with fewer failures occurring.

In addition to producing comparative amounts of sediment between estimated and modeled loads, the model also simulates a similar response in sediment mobilized in the watershed. The vertical pulses seen in Figure 9 are indicative of flow events that resulted in increased mobilization of sediment. The observed loads show only small contributions of sediment during periods of low flow. The modeled loads show a similar response overall, with relatively low amounts of sediment being mobilized during low flow periods. In 2014, the model does not capture pulses of sediment that likely occurred as a result of small precipitation and flow events (Figure 9b). The model can be parameterized to capture more mobilization of sediment at low flows, however, this results in a large overestimation of sediment at higher flows. The results of the coupled model do however show improved overall estimation of cumulative sediment as compared to the model with BSTEM inactivated (original DHSVM), particularly in 2013 where more frequent and high magnitude precipitation events occurred than in 2014.

Another goal for simulating sediment was to represent realistic proportions of sediment mobilized by overland erosion, road erosion, and stream bank erosion. Few studies have quantified sediment loading

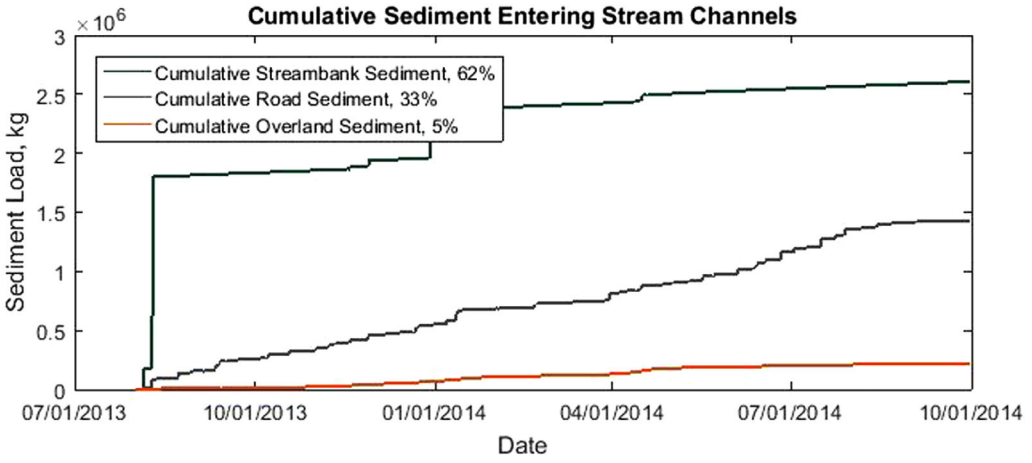

Figure 10. Cumulative proportions of simulated sediment mobilized by overland erosion, road erosion, and stream bank erosion and entering stream channel network throughout Mad River watershed.

resulting from stream bank or road erosion in Vermont watersheds. Studies typically report considerable variability in those estimates, particularly with respect to stream bank erosion among different reaches [*DeWolfe et al*., 2004; *Morrissey et al*., 2011; *Langendoen et al*., 2012]. Despite this variability, we used these prior studies as a general basis for approximating relative proportions of sediment being generated from overland erosion, stream bank erosion, and erosion of roads. The Mad River watershed is largely forested, so overland erosion was expected to be relatively low in comparison to other watersheds where urban and agricultural land uses may dominate. Figure 10 shows total sediment mobilized and entering the stream channel network within the entire watershed by the three mechanisms previously mentioned. On average, stream bank erosion and failure generated approximately 62% of total sediment load during the modeled time period, road erosion produced 33%, and overland erosion produced the remaining 5%. For this calibration, the proportion of sediment mobilized by each source only varied within $\pm$4% of the average of these 10 results. These estimates fall within the range of estimates of the contribution of stream banks to overall sediment loading from studies such as those cited above. Again the behavior of sediment mobilization by stream bank erosion/failure is also apparent in this plot, where cumulative sediment increases in pulses that correspond to precipitation and/or high flow events.

Further examination of model-generated sediment by these three sources shows that these proportions show logical variability between subbasins. Although we could not output total sediment mobilized throughout each of the subbasins, we could look at the makeup of suspended sediment at the outlet of the subbasins. These results are different from those presented above in that they are impacted by sediment transport processes. Heavier particles are allowed to settle out in stream segments where velocity and stream power decline. Therefore, the relative proportions of sediment in subbasin outlets, and particularly at the outlet of the watershed at Moretown, differ from the original proportions of total sediment mobilized within the watershed. Total cumulative suspended sediment was calculated for these subbasins using the modeled suspended sediment concentration at each outlet, the corresponding outlet discharge, and the tracked ratio of stream bank, road, and overland erosion that is outputted at each time step and each location. Figure 11 shows the cumulative suspended sediment from overland erosion, roads, and stream banks at the outlet of the watershed, as well as at each of the five subbasin outlets. In addition, Table 3 presents a comparison of model simulated road erosion results to estimates made by *Wemple* [2013]. The model predicts significantly less suspended sediment from roads than was estimated by *Wemple*, although the overall amount generated is the same order of magnitude as her lower bound estimates. *Wemple* estimated TSS from roads based on annually scaled suspended flux measurements during specific storm events, most of which occurred in the summer and fall months of 2011, as well as in spring and summer of 2012. However, these years received more precipitation and higher flow events were observed in these time periods (particularly late 2011) than in 2014. Therefore, it was expected that the amount of sediment generated by road erosion would be less in the 2014 water year. The range of percent contributions of roads in these

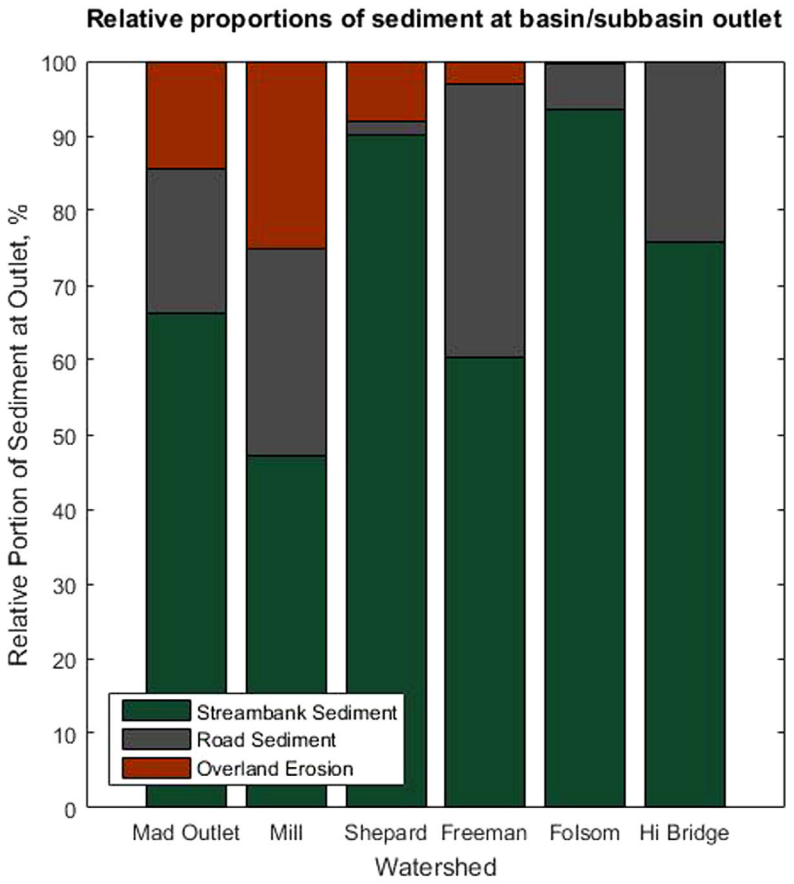

Figure 11. Relative proportions of simulated cumulative suspended sediment at Mad River and subbasin outlets.

subbasins are similar however, indicating that the model is capable of representing realistic estimations of the proportions of suspended sediment from this mechanism.

Without field data to compare absolute contributions of suspended sediment from stream bank and overland erosion, we also looked at the relative contributions of these mechanisms with respect to land characteristics of those subbasins. Table 2 lists relative characteristics of these subbasins, such as the road-to-stream length ratios and percent coverage of land cover types. Freeman and High Bridge subbasins have the highest road-to-stream ratios as well as the highest percentage of land use classified as roads, which is reflected in higher proportions of sediment from road erosion in these subbasins (37% and 24%, respectively) than in other watersheds. The largest percentages of sediment from overland erosion at outlet locations occurred in Mill Brook and Shepard Brook, which were also the largest subwatersheds (Table 2) and had the largest ranges of elevation. The contribution of sediment from overland erosion was very negligible in small upland subwatersheds (<1% in Folsom and High Bridge).

Table 3. Comparison of Road Sediment

	Mill Brook Subbasin	Shepard Brook Subbasin	Freeman Brook Subbasin	Folsom Brook Subbasin	High Bridge Subbasin
Wemple [2013] estimate of road TSS production (kg/yr)	330,265	204,212	145,054	75,816	90,664
Wemple [2013] lower bound estimate of road TSS production (kg/yr)	13,513	8,387	6,060	3,209	3,821
Model predicted road TSS production (kg/2014 water year)	8,693	1,159	9,032	1,191	1,564
Wemple [2013] estimate of contribution of roads to catchment TSS load (%)	27.2	19.9	12.7	9.9	11.4
Model predicted contribution of roads to catchment TSS load (%)	11.4	20.1	36.7	6.4	24.3

5. Discussion and Conclusions

5.1. Model Capability and Performance

This work presents a new capability in an existing watershed model for simulation of sediment generation within a spatially explicit environment. By coupling a watershed and bank stability model, we can more inclusively represent the processes that mobilize sediment, including the erosion and particularly failure of stream banks, which were previously not present in similar distributed models but represent important sediment mobilization processes in many watersheds. Overall the stream bank erosion processes are captured in the coupled model approach, with some limitations. Comparison with available field data indicates that the coupled model simulates the approximate magnitude and timing of sediment mobilization in the watershed and its subbasins, however generally underestimates suspended sediment concentrations resulting from relatively small storm/flow events. Despite differences in the resolution of model and field data, it was evident that the coupled model still improved prediction of cumulative loads and in some cases suspended sediment concentrations in association with elevated flow events in comparison to the simulation conducted without representation of these processes. The coupled model also logically represents watershed characteristics that would impact erosion processes, such as land use, slope, and vegetation.

Although several sites were monitored for bank erosion and failure, no instances of mass failure occurred during the modeled time period so no comparison or analysis of specific failure events could be made in this work. The 2014 water year was relatively dry with few events that elevated flow other than spring melt. Midwinter thaws that occurred during January 2014 were reflected in sediment results, where precipitation that occurred during these periods was modeled as rain on snow events. Temperatures above freezing resulted in snow melting, elevated flow conditions, and the occurrence of bank failures as expected. Elevated erosion and small failures also occurred during flows associated with the spring melt and were likely a result of bank undercutting during this period. No significant precipitation coincided with this spring period. Also, no data related to suspended sediment, erosion, or failures were available during the winter or spring melt period.

This application of DHSVM represents a scaling up of the use of this hydrological model from small headwater watersheds to larger watersheds where bank erosion may play a bigger role. With some exceptions, much of the work using DHSVM has been conducted on watersheds of less than 50 km^2 [e.g., *Wigmosta and Lettenmaier*, 1999; *Bowling and Lettenmaier*, 2001; *Waichler et al*., 2005; *Doten et al*., 2006; *Surfleet et al*., 2010; *Du et al*., 2014]. In larger watersheds, particularly those where the landscape has been modified in ways that increase stream channel instability (such as deforestation, agriculture, and urban development), simulation of the processes contributing to bank erosion and failure will generate a more complete picture of how sediment is mobilized and transported. The influence of local meteorological data, particularly precipitation, is also clear in the application of this modeling approach. Particularly in larger watersheds and watersheds with large ranges in elevation, the impact of local storms and spatial variability in rainfall may have an important impact on sediment mobilization processes. The model time step used in this work (2 h) was chosen based on the limited availability of higher resolution data for all variable needed to drive the hydrology model. Inclusion of high spatial resolution precipitation data could improve model performance, particularly with respect to water table conditions and lag times.

5.2. Supply/Transport Limit Conditions

Results indicated that there was generally more sediment available than transport capacity to move that sediment during relatively low flow events. This was reflected in similar suspended sediment concentrations predicted by the model at low flows, with and without BSTEM activated. Changes in parameter values that increased available sediment resulted in no changes in the low flow, subbasin sediment concentration values. The years for which we have data on suspended sediment in the watershed were relatively dry, with no significant precipitation or high flow events. It was therefore difficult to assess model performance under conditions where large amounts of sediment would be mobilized by bank failures and high flow conditions would allow transport of that material. The variability in results due to probabilistic parameter assignment was seen primarily in the magnitude of sediment pulse events, where the number of failures showed some variability, but typically occurred within the same few time steps. This was reflected in higher peaks in suspended sediment concentrations at relatively higher flows, however, no difference was seen with low flow

events. The results presented here indicate the potential for this approach to improve our ability to simulate sediment mobilization and transport under higher flow conditions.

5.3. Insight Into Sources of Sediment

Results indicate that in the Mad River watershed, where the landscape is largely forested and surface erosion is minimal, stream bank erosion and failure were major contributors of sediment to streams and receiving waters between 1 August 2013 and 30 September 2014. Differences in the relative proportions of suspended sediment originating from stream bank, road, and overland erosion at subbasin outlets are indicative of factors such as land use and channel characteristics impacting the simulation of those processes. Previous studies conducted in Vermont watersheds have large ranges of sediment proportion generated by stream bank erosion and failure. For example, *Morrissey et al*. [2011] estimated that on a reach basis, stream bank erosion accounted for 15–80% of total eroded sediment. *Langendoen et al*. [2012] used BSTEM to estimate sediment loading from stream bank erosion in an agricultural watershed in Vermont and found that 36% of total suspended sediment leaving the watershed was from stream bank erosion. Specific to the Mad River watershed, *Wemple* [2013] estimated that unpaved roads contribute 10–27% of the annual sediment yield from the five subbasins used in this study. The coupled model presented here generated suspended sediment loads that agreed well with these field-based estimates. Model results indicated that road sediment contributed 10–37% of sediment seen at these same subbasin outlets. Additionally, in this study, roads contributed 33% of simulated mobilized sediment that reached stream networks in the watershed, which also compared well to field-based estimates for annual average suspended sediment from roads for the Mad River and Winooski watersheds (17–31%) [*Wemple*, 2013]. However, 19% of simulated suspended sediment at the watershed outlet near Moretown originated as road sediment. It may be that much of the road sediment from upstream subbasins was redeposited in slower stream segments before reaching the outlet of the watershed. This deposition of road sediment is related to the larger particle size of road sediment. Road sediment particle size was set larger than stream bank sediment. It therefore falls into a larger sediment bin size which the model transports with remaining stream power once smaller sediment has been moved. Overland sediment was parameterized as finer particles, and although overland erosion was only 5% of total sediment mobilized, 14% of sediment seen at the outlet originated from this source, indicating that these particles remained in suspension.

5.4. Parameter Sensitivity

An increase in the number of failures occurring, the amount of sediment mobilized, and thereby suspended sediment concentrations in the stream channels, can be achieved by adjusting relevant parameters such as cohesion, radius of curvature, and critical shear stress. However, this also results in an increase in suspended sediment concentration during base flow conditions, indicating an overestimation of continuous erosion of banks, and ultimately leading to overestimation of cumulative suspended sediment. This could potentially be addressed by delineating the stream network into smaller segments or using a smaller grid size (grid cells here were 100 m by 100 m), but maintaining variability among reaches, so that segments where erosion and failures occur frequently, a smaller volume of sediment is being contributed to the overall system. In this work, erosion calculated on any stream segment was applied to half the length of the channel segment contained in that grid cell. This may be relatively accurate if using a small grid cell size, however, the coarser the resolution of the model, the less likely this assumption is to realistically represent actual erosion. Alternatively, the model could be modified so that the volume of sediment lost due to the rate of erosion or a mass failure was calculated based on a smaller portion of that stream segment, perhaps as a function of the radius of curvature. This fraction of the stream reach to which erosion and failure is applied should be treated as a user-defined calibration and further investigation could attempt to identify a physically based method for assessing this value.

Along with the above mentioned modifications, this approach would also be improved by future efforts to improve the ability of the model to represent changes in the position of the channels in the landscape and associated changes in sinuosity. The model currently does not modify landscape processes in response to channel erosion and migration. In addition, as continuous erosion occurs, sinuosity and radius of curvature of that stream segment would be altered. Although we believe this approach has great potential for use in investigating the impacts of climate and land use change, improvements in this area would further improve the suitability of this approach, particularly for long-term (decadal to century time scale) simulations.

5.5. Sediment Tracking

The ratio used to track stream bank sediment was calculated based on the influxes to each stream segment and then applied to sediment leaving that segment. This was considered a valid assumption since those ratios are calculated and tracked for each model sediment bin size. Once sediment is added to a bin size in DHSVM, it is not further differentiated in the model. Sediment from all sources (roads, streams, overland, and debris flow) entering a stream segment are combined, as well as sediment mass stored in that segment, the total transport capacity is calculated and some portion of the total available sediment is moved to the next segment. Remaining sediment that is in excess of the total transport capacity is redeposited in that segment and available for transport at the next time step. No preference is given to transporting already suspended sediment over stored/settled sediment in any segment. In reality however, currently suspended sediment is more likely to be transported than stored sediment and the ratio of stream bank sediment to other sediment entering a reach is not necessarily the same as the ratio at the reach outlet. In the current parameterization, a significant portion of road sediment is redeposited before reaching the outlet because of coarser particle size, whereas sediment from overland erosion is more easily transported due to incipient motion on the land surface favoring fines. Stream bank soils are represented mostly as silty loams and loamy sands, which are between road and overland sediment particle sizes. The high proportions of stream bank soils seen in these results are also affected by the locations chosen for model comparison. Most simulated stream bank erosion and failure occurs along the lower portion of the main stem and to some extent along major tributaries of the Mad River, so these sediments are transported shorter distances to locations where model results are compared to field data.

5.6. Limitations and Suggestions for Future Work

This approach could be further improved to better represent the physical conditions and processes contributing to sediment mobilization, in particular from bank erosion and failure. For example, recent version of BSTEM incorporates the occurrence and impact of tension cracks on bank stability. In Vermont, tension cracks are not a commonly seen mode of failure and so were not incorporated in this work. However, in other regions, this may have a more pronounced impact on bank stability and further work could enhance the model by incorporating those processes. Additionally, BSTEM includes a RIP ROOT module [*Pollen and Simon*, 2005], that calculates the specific additional cohesion due to roots on bank stability forces. Additional work could enhance the ability to simulate specific bank vegetation or bank stability measures in a spatially explicit format.

Bedrock outcroppings in the Mad River Valley constrict the river and cause ponding during heavy precipitation events. Slower velocities lead to sediment deposition and bank erosion where flow is diverted. Sediment in tributaries as well as the main stem is then periodically flushed out by large events. This ponding effect is difficult to model, but could potentially be achieved by manual delineation and description of the stream network. This was not attempted for this work but may be an avenue for future research. Using a stream network that more accurately describes explicit changes in widths and slopes of stream segments should allow the model to produce more accurate estimates of stream power, which could potentially be investigated as an indicator of erosional hot spots similar to how *Gartner et al*. [2015] identified hot spots using a logistic regression model based on channel slope, curvature, and length of upstream segment.

5.7. Implications

The importance of simulating stream bank failures is partly because sediment can be a water quality issue in its own right, but also because bound phosphorus can contribute significantly to nutrification problems in receiving water bodies, such as Lake Champlain which suffers excess nutrient loads that lead to eutrophication and harmful algal blooms. *Ishee et al*. [2015] suggested that landscape position (floodplain, low slope versus upland soil) may be useful in identifying stream bank erosion sites where soils are more likely to have higher total phosphorus (TP) concentrations [*Ishee et al*., 2015]. However, although TP is often used as an index of P loading, these authors also suggested, based on lower concentrations of Morgan Modified P (MM P) and degree of phosphorus saturation (DPS), that eroding stream bank soils may actually act as phosphorus sinks, contrary to prior conclusions. This suggests that more work is needed to qualify stream bank erosion based on bioavailable phosphorus measures in order to assess the impact on nutrient loading.

The presented coupled model advances mechanistic representation of suspended sediment within a watershed. Such modeling ability is valuable for simulating the potential impacts of climate and land use changes

on sediment and nutrient budgets as precipitation driving flood events continues to become more extreme. Because we expect higher intensity precipitation events would likely have a larger impact on stream bank erosion and failure, this coupling may be particularly beneficial for simulating extreme event and climate change scenarios. Although we did not have data available for validating model performance under extreme precipitation conditions, this approach shows the potential to better represent watershed response to such conditions than other similar watershed models. In this work, we saw the most significant differences in suspended sediment concentrations between the original DHSVM and the coupled DHSVM-BSTEM model under elevated flow conditions, as well as with the occurrence of winter thaw events. The ability to more inclusively simulate the processes that mobilize sediment from a watershed has important implications for water quality assessment and related policy issues (such as climate adaptation). The physics-based nature of this coupled modeling approach will be particularly well suited for assessing the potential impacts of future shifts in climate and land use on water quality and land management.

Acknowledgments
This research was supported by the Vermont Experimental Program for Stimulating Competitive Research (EPSCoR) and funded by NSF award EPS #1101317, Research on Adaptation to Climate Change in the Lake Champlain Basin (RACC). The authors are grateful to a number of people involved in the RACC project. Colleagues Kristen Underwood, Scott Hamshaw, as well as undergraduate student intern Sean Brennan, made invaluable contributions to the field work and data collection for this study. In addition, many thanks to Eddy Langendoen and the U.S. Department of Agriculture, Agricultural Research Service, National Sedimentation Laboratory (USDA-ARS, NSL) for sharing an open version of BSTEMv5.4 with us. The data used are listed in the references, tables, figures, supporting information and are further available by contacting the corresponding author.

References

Aksoy, H. and M. L. Kavvas (2005), A review of hillslope and watershed scale erosion and sediment transport models, *Catena*, *64*(2), 247–271.

Barg, L., and M. Blazewicz (2003), *Assessment of Fluvial Geomorphology in Relation to Erosion and Landslides in the Mad River Watershed in Central Vermont*, Prepared for Vermont Geological Survey, Friends of the Mad River.

Bathurst, J. C. (2002), Physically-based erosion and sediment yield modelling: The SHETRAN concept, in *Modelling Erosion, Sediment Transport and Sediment Yield*, UNESCO International Hydrological Programme, 47 pp.

Bathurst, J. C., G. Moretti, A. El-Hames, A. Moaven-Hashemi, and A. Burton (2005), Scenario modelling of basin-scale, shallow landslide sediment yield, Valsassina, Italian Southern Alps, *Nat. Hazards Earth Syst. Sci.*, *5*(2), 189–202.

Beeler, K. B. (2014), Sediment and phosphorus inputs from perennial streams to Lake Whatcom, northwestern Washington State, MS Thesis, West. Wash. Univ., Bellingham.

Berry, W., N. Rubenstein, and B. Melzian (2003), The biological effects of suspended and bedded sediment (SABS) in aquatic systems: A review, United States Environmental Protection Agency internal report, Office of Research and Development, National Health and Environmental Effects Laboratory, Midcontinent Ecology Division, Duluth, Minn.

Bilotta, G. S., and R. E. Brazier (2008), Understanding the influence of suspended solids on water quality and aquatic biota, *Water Res.*, *42*(12), 2849–2861, doi:10.1016/j.watres.2008.03.018.

Birkinshaw, S. J., and J. C. Bathurst (2006), Model study of the relationship between sediment yield and river basin area, *Earth Surf. Processes Landforms*, *31*(6), 750–761, doi:10.1002/esp.1291.

Bowling, L. C., and D. P. Lettenmaier (2001), The effects of forest roads and harvest on catchment hydrology in a mountainous maritime environment, in *Land Use and Watersheds: Human Influence on Hydrology and Geomorphology in Urban and Forest Areas*, edited by M. S. Wigmosta and S. J. Burges, pp. 145–164, AGU, *Water Science and Application Series* (No. PNNL-SA-31836), Northwest National Laboratory (PNNL), Richland, Wash.

Clement, C. R. (2014), Estimating sediment yield from the Swift Creek landslide, Whatcom County, Washington State, MS Thesis, West. Wash. Univ., Bellingham.

Cuo, L., D. P. Lettenmaier, B. V. Mattheussen, P. Storck, and M. Wiley (2008), Hydrologic prediction for urban watersheds with the Distributed Hydrology–Soil–Vegetation Model, *Hydrol. Processes*, *22*(21), 4205–4213, doi:10.1002/hyp.7023.

Cuo, L., D. P. Lettenmaier, M. Alberti, and J. E. Richey (2009), Effects of a century of land cover and climate change on the hydrology of the Puget Sound basin, *Hydrol. Processes*, *23*(6), 907–933, doi:10.1002/hyp.7228.

Cuo, L., T. W. Giambelluca, and A. D. Ziegler (2011), Lumped parameter sensitivity analysis of a distributed hydrological model within tropical and temperate catchments, *Hydrol. Processes*, *25*(15), 2405–2421, doi:10.1002/hyp.8017.

Darby, S. E., C. R. Thorne, and A. Simon (1996), Numerical simulation of widening and bed deformation of straight sand-bed rivers .2. Model evaluation, *J. Hydraul. Eng.*, *122*(4), 194–202, doi:10.1061/(ASCE)0733-9429(1996)122:4(194).

DeWolfe, M., W. Hession, and M. Watzin (2004), Sediment and phosphorus loads from streambank erosion in Vermont, USA, *Crit. Trans. Water Environ. Resour. Manage.*, *436*, 1–10.

Doten, C. O., L. C. Bowling, J. S. Lanini, E. P. Maurer, and D. P. Lettenmaier (2006), A spatially distributed model for the dynamic prediction of sediment erosion and transport in mountainous forested watersheds, *Water Resour. Res.*, *42*, W04417, doi:10.1029/2004WR003829.

Du, E., T. E. Link, J. A. Gravelle, and J. A. Hubbart (2014), Validation and sensitivity test of the distributed hydrology soil-vegetation model (DHSVM) in a forested mountain watershed, *Hydrol. Processes*, *28*(26), 6196–6210, doi:10.1002/hyp.10110.

Duan, J. G., S. S. Y. Wang, and Y. Jia (2001), The applications of the enhanced CCHE2D model to study the alluvial channel migration processes, *J. Hydraul. Res.*, *39*(5), 469–480, doi:10.1080/00221686.2001.9628272.

Dunn, R. K., G. E. Springston, and N. Donahue (2007a), *Surficial Geologic Map of the Mad River Watershed, Vermont (Northern Sheet)*, Vermont Agency of Natural Resources.

Dunn, R. K., G. E. Springston, and N. Donahue (2007b), *Surficial Geology Map of the Mad River Watershed, Vermont (Southern Sheet)*, Vermont Agency of Natural Resources.

European Environment Agency (1995), *European Rivers and Lakes—Assessment of Their Environmental State, EEA Environ. Monogr*.

Evans, D. J., C. E. Gibson, and R. S. Rossell (2006), Sediment loads and sources in heavily modified Irish catchments: A move towards informed management strategies, *Geomorphology*, *79*(1–2), 93–113, Office for Official Publications of the European Union, Luxembourg, doi:10.1016/j.geomorph.2005.09.018.

Ewen, J., G. Parkin, and P. E. O'Connell (2000), SHETRAN: Distributed river basin flow and transport modeling system, *J. Hydrol. Eng.*, *5*(3), 250–258, doi:10.1061/(ASCE)1084-0699(2000)5:3(250).

Field Geology Services (2007), *Fluvial Geomorphology Assessment of the Mad River Watershed, Vermont, Mad River Geomorphic Assessment*, Vermont Agency of Nat. Resour. Montpelier, Vermont.

Fitzgerald, E. P. and L. C. Godfrey (2008), Upper Mad River Corridor Plan, Prepared for Friends of the Mad River, Waitsfield, Vermont, Retrieved from Vermont Agency of Natural Resources. [Available at https://anrweb.vt.gov/DEC/SGA/finalReports.aspx.]

Foster, D. R., and J. D. Aber (Eds.) (2004), *Forests in Time: The Environmental Consequences of 1000 Years of Change in New England*, Yale Univ. Press, New Haven, Conn.
Gartner, J. E., P. M. Santi, and S. H. Cannon (2015), Predicting locations of post-fire debris-flow erosion in the San Gabriel Mountains of southern California, *Natural Hazards*, *77*(2), 1305–1321, doi:10.1007/s11069-015-1656-3.
Guilbert, J., A. K. Betts, D. M. Rizzo, B. Beckage, and A. Bomblies (2015), Characterization of increased persistence and intensity of precipitation in the northeastern United States, *Geophys. Res. Lett.*, *42*, 1888–1893, doi:10.1002/2015GL063124.
Hamshaw, S. (2014), *Suspended Sediment Prediction Using Artificial Neural Networks and Local Hydrometeorological Data*, Univ. of Vermont, Burlington.
Hanson, G. J. (1990), Surface erodibility of earthen channels at high stresses: Developing an in situ testing device, *Trans. Am. Soc. Agric. Eng.*, *33*, 132–137.
Hanson, G. J. and A. Simon (2001), Erodibility of cohesive streambeds in the loess area of the midwestern USA, *Hydrological Processes*, *15*(1), 23–38, doi:10.1002/hyp.149.
Huang, D. (2012), Quantifying stream bank erosion and deposition rates in a central U.S. urban watershed, thesis, Univ. of Mo., Columbia.
Ishee, E. R., D. S. Ross, K. M. Garvey, R. R. Bourgault, and C. R. Ford (2015), Phosphorus characterization and contribution from eroding streambank soils of Vermont's Lake Champlain Basin, *J. Environ. Qual.*, *44*(6), 1745–1753, doi:10.2134/jeq2015.02.0108.
Karl, T. R., J. M. Melillo, and T. C. Peterson (2009), *Global Climate Change Impacts in the United States, U.S. National Climate Assessment, United States Global Change Research Program*, Cambridge Univ. Press, New York.
Kleinman, P., A. Sharpley, A. Buda, R. McDowell, and A. Allen (2011), Soil controls of phosphorus in runoff: Management barriers and opportunities, *Can. J. Soil Sci.*, *91*(3), 329–338.
Kline, M., and B. Cahoon (2010), Protecting river corridors in Vermont, *J. Am. Water Resour. Assoc.*, *46*, 227–236. doi:10.1111/j.1752-1688.2010.00417.x.
Kronvang, B., R. Grant, and A. L. Laubel (1997a), Sediment and phosphorus export from a lowland catchment: Quantification of sources, *Water Air Soil Pollut.*, *99*(1–4), 465–476.
Kronvang, B., A. Laubel, and R. Grant (1997b), Suspended sediment and particulate phosphorus transport and delivery pathways in an arable catchment, Gelbaek Stream, Denmark, *Hydrol. Processes*, *11*(6), 627–642, doi:10.1002/(SICI)1099-1085(199705)11:6 < 627::AID-HYP481 > 3.0.CO;2-E.
Langendoen, E. J. (2000), *CONCEPTS—Conservational Channel Evolution and Pollutant Transport System: Stream Corridor Version 1.0*, U.S. Dep. of Agric., Agric. Res. Serv., Natl. Sedimentation Lab., Oxford, Miss.
Langendoen, E. J. (2001), CONCEPTS—A process-based modeling tool to evaluate stream-corridor restoration designs, paper presented at the 2001 Wetlands Engineering & River Restoration Conference, August 27-31, edited by D. F. Hayes, Am. Soc. of Civ. Eng., Reston, Va.
Langendoen, E. J., A. Simon, A. Curini, and C. V. Alonso (1999), Field validation of an improved process-based model for streambank stability analysis, paper presented at 1999 International Water Resources Engineering Conference, edited by R. Walton and R. E. Nece, Am. Soc. of Civ. Eng., Reston, Va.
Langendoen, E. J., A. Simon, and C. V. Alonso (2000), Modeling channel instabilities and mitigation strategies in eastern Nebraska, paper presented at the Joint Conference on Water Resource Engineering and Water Resources Planning and Management 2000, edited by R. H. Hotchkiss and M. Glade, Am. Soc. of Civ. Eng., Reston, Va.
Langendoen, E. J., A. Simon, L. Klimetz, N. Bankhead, and M. E. Ursic (2012), Quantifying sediment loadings from streambank erosion in selected agricultural watersheds draining to Lake Champlain, NSL Technical Report No. 79, U.S. Dep. of Agric. Natl. Sedimentation Lab, Oxford, Mississippi.
Laubel, A., L. M. Svendsen, B. Kronvang, and S. E. Larsen (1999), Bank erosion in a Danish lowland stream system, *Hydrobiologica*, *410*, 279–285.
Legates, D. R., and G. J. McCabe (1999), Evaluating the use of "goodness-of-fit" measures in hydrologic and hydroclimatic model validation, *Water Resour. Res.*, *35*(1), 233–241, doi:10.1029/1998WR900018.
Leung, L. R., and M. S. Wigmosta (1999), Potential climate change impacts on mountain watersheds in the Pacific Northwest, *J. Am. Water Resour. Assoc.*, *35*(6), 1463–1471, doi:10.1111/j.1752-1688.1999.tb04230.x.
Lukey, B. T., J. Sheffield, J. C. Bathurst, R. A. Hiley, and N. Mathys (2000), Test of the SHETRAN technology for modelling the impact of reforestation on badlands runoff and sediment yield at Draix, France, *J. Hydrol.*, *235*(1–2), 44–62, doi:10.1016/S0022-1694(00)00260-2.
Merritt, W. S., R. A. Letcher, and A. J. Jakeman (2003), A review of erosion and sediment transport models, *Environ. Modell. Software*, *18*(8–9), 761–799, doi:10.1016/S1364-8152(03)00078-1.
Midgley, T. L., G. A. Fox, and D. M. Heeren (2012), Evaluation of the Bank Stability and Toe Erosion Model (BSTEM) for predicting lateral retreat on composite streambanks, *Geomorphology*, *145–146*, 107–114, doi:10.1016/j.geomorph.2011.12.044.
Morrissey, L. A., D. M. Rizzo, D. S. Ross, and C. Alves (2011), *Quantifying Sediment Loading Due To Stream Bank Erosion in Impaired and Attainment Watersheds in Chittenden County, VT Using Advanced GIS and Remote Sensing Technologies*, Project ID 2009VT44B U.S. Geol. Surv.
Nagata, N., T. Hosoda, and Y. Muramoto (2000), Numerical analysis of river channel processes with bank erosion, *J. Hydraul. Eng.*, *126*(4), 243–252, doi:10.1061/(ASCE)0733-9429(2000)126:4(243).
Nagle, G. N., T. J. Fahey, J. C. Ritchie, and P. B. Woodbury (2007), Variations in sediment sources and yields in the Finger Lakes and Catskills regions of New York, *Hydrol. Processes*, *21*(6), 828–838, doi:10.1002/hyp.6611.
Nash, J. E., and J. V. Sutcliffe (1970), River flow forecasting through conceptual models: Part I—A discussion of principles, *J. Hydrol.*, *10*(3), 282–290.
National Weather Service (2011), Public Information Statement, Spotter Reports, Burlington, Vermont.
Nebel, B. J., and R. T. Wright (1993), Impacts of sediments on streams and rivers, in *Environmental Science: The Way the World Works*, pp. 281–283, Prentice Hall, Englewood Cliffs, N. J.
Paerl, H. W., N. S. Hall, and E. S. Calandrino (2011), Controlling harmful cyanobacterial blooms in a world experiencing anthropogenic and climatic-induced change, *Sci. Total Environ.*, *409*(10), 1739–1745, doi:10.1016/j.scitotenv.2011.02.001.
Parker, S. P., E. P. Fitzgerald, and L. C. Godfrey (2008), Mad River Headwaters Phase 2 Stream Geomorphic Assessments, Prepared for Friends of the Mad River, Waitsfield, VT. [Available at https://anrweb.vt.gov/DEC/SGA/finalReports. aspx, retrieved from Vermont Agency of Natural Resources.]
Pollen, N., and A. Simon (2005), Estimating the mechanical effects of riparian vegetation on stream bank stability using a fiber bundle model, *Water Resour. Res.*, *41*, W07025, doi:10.1029/2004WR003801.
Schindler, D. W., R. E. Hecky, D. L. Findlay, M. P. Stainton, B. R. Parker, M. J. Paterson, K. G. Beaty, M. Lyng, and S. E. M. Kasian (2008), Eutrophication of lakes cannot be controlled by reducing nitrogen input: Results of a 37-year whole-ecosystem experiment, *Proc. Natl. Acad. Sci. U. S. A.*, *105*(32), 11,254–11,258, doi:10.1073/pnas.0805108105.

Schumm, S. A., Harvey, M. D., Watson, C. C. (1984), *Incised Channels, Morphology, Dynamics and Control*, 200 pp., Water Resources Publications, Littleton, Colo.
Sekely, A. C., D. J. Mulla, and D. W. Bauer (2002), Streambank slumping and its contribution to the phosphorus and suspended sediment loads of the Blue Earth River, Minnesota, *J. Soil Water Conserv.*, *57*(5), 243–250.
Sharpley, A. N., S. C. Chapra, R. Wedepohl, J. T. Sims, T. C. Daniel, and K. R. Reddy (1994), Managing agricultural phosphorus for protection of surface waters: Issues and options, *J. Environ. Qual.*, *23*(3), 437, doi:10.2134/jeq1994.00472425002300030006x.
Sharpley, A. N., M. J. Hedley, E. Sibbesen, A. Hillbricht-Ilkowska, W. A. House, and L. Ryskowski (1995), Phosphorus transfers from terrestrial to aquatic ecosystems, in *Phosphorus in the Global Environment*, pp. 171–199, edited by H. Tiessen, Wiley, N. Y.
Simon, A. (1989), A model of channel response in disturbed alluvial channels, *Earth Surf. Processes Landforms*, *14*(1), 11–26, doi:10.1002/esp.3290140103.
Simon, A. (1995), Adjustment and recovery of unstable alluvial channels: Identification and approaches for engineering management, *Earth Surf. Processes Landforms*, *20*(7), 611–628, doi:10.1002/esp.3290200705.
Simon, A., A. Curini, S. E. Darby, and E. J. Langendoen (2000), Bank and near-bank processes in an incised channel, *Geomorphology*, *35*(3–4), 193–217.
Simon, A., E. J. Langendoen, and R. Thomas (2003), *Incorporating Bank-Toe Erosion by Hydraulic Shear into a Bank-Stability Model: Missouri River, Eastern Montana*. pp. 70–76, First Interagency Conference on Research in the Watersheds. USDA ARS, Benson, Ariz.
Simon, A., E. Langendoen, R. Bingner, R. Wells, Y. Yuan, C. Alonso (2004), Suspended-sediment transport and bed-material characteristics of Shades Creak, Alabama and Ecoregion 67: Developing water-quality criteria for suspended and bed-material sediment, *Tech. Rep. 43*, U.S. Dep. of Agric.-Agric. Res. Serv., Natl. Sedimentation Lab, USDA ARS.
Simon, A., N. Pollen, and E. Langendoen (2006), Influence of two woody riparian species on critical conditions for streambank stability: Upper Truckee River, California, *J. Am. Water Resour. Assoc.*, *42*(1), 99–113, doi:10.1111/j.1752-1688.2006.tb03826.x.
Simon, A., N. Pollen-Bankhead, and R. E. Thomas (2011), Development and application of a deterministic Bank Stability and Toe Erosion Model for stream restoration, in *Stream Restoration in Dynamic Fluvial Systems*: *Scientifica Approaches, Analyses and Tools*, edited by A. Simon, S. J. Bennett, and J. M. Castro, pp. 453–474.
Søndergaard, M., J. P. Jensen, and E. Jeppesen (2003), Role of sediment and internal loading of phosphorus in shallow lakes, *Hydrobiologia*, *506–509*(1–3), 135–145, doi:10.1023/B:HYDR.0000008611.12704.dd.
Stanners, D., P. Bourdeau, and European Environment Agency (1995), *Europe's Environment: The Dobrís Assessment*, European Environment Agency. [Available at http://bases.bireme.br/cgi-bin/wxislind.exe/iah/online/?IsisScript=iah/iah.xis&src=google&base=REPIDISCA&lang=p&nextAction=lnk&exprSearch=56027&indexSearch=ID.]
Storck, P., L. Bowling, P. Wetherbee, and D. Lettenmaier (1998), Application of a GIS-based distributed hydrology model for prediction of forest harvest effects on peak stream flow in the Pacific Northwest, *Hydrol. Processes*, *12*(6), 889–904, doi:10.1002/(SICI)1099-1085(199805)12:6 < 889::AID-HYP661 > 3.0.CO;2-P.
Surfleet, C. G., A. E. Skaugset, and J. J. McDonnell (2010), Uncertainty assessment of forest road modeling with the Distributed Hydrology Soil Vegetation Model (DHSVM), *Can. J. For. Res.*, *40*(7), 1397–1409, doi:10.1139/X10-079.
US EPA (2000), *1998 National Water Quality Inventory Report to Congress*, Washington, D. C. [Available at http://www.epa.gov/waterdata/1998-national-water-quality-inventory-report-congress.]
US EPA (2002), *2000 National Water Quality Inventory*, Washington, D. C. [Available at http://water.epa.gov/lawsregs/guidance/cwa/305b/2000report_index.cfm.]
US EPA (2015), *Developing Water Quality Criteria for Suspended and Bedded Sediments (SABs)*. Washington, D. C. [Available at https://www.epa.gov/wqc/developing-water-quality-criteria-suspended-and-bedded-sediments-sabs.]
Vörösmarty, C. J., et al. (2010), Global threats to human water security and river biodiversity, *Nature*, *467*(7315), 555–561, doi:10.1038/nature09440.
Waichler, S. R., B. C. Wemple, and M. S. Wigmosta (2005), Simulation of water balance and forest treatment effects at the H.J. Andrews experimental forest, *Hydrol. Processes*, *19*, 3177–3199.
Walter, R. C., and D. J. Merritts (2008), Natural streams and the legacy of water-powered mills, *Science*, *319*(5861), 299–304, doi:10.1126/science.1151716.
Wang, H., G. Zhou, and X. J. Shao (2010), Numerical simulation of channel pattern changes. Part I: Mathematical model, *Int. J. Sediment Res.*, 4, 366–378.
Waters, T. F. (1995), *Sediment in Streams—Sources, Biological Effects and Control, Am. Fish. Soc. Monogr. 7*, Am. Fish. Soc., Bethesda, Md.
Wemple, B. (2013), Assessing the effects of unpaved roads on Lake Champlain water quality, Technical Report No. 74, Grand Isle, Vermont.
Whalen, T. N. (1998), Post-glacial fluvial terraces in the Winooski Drainage Basin, Vermont, MS thesis, Univ. of Vermont, Burlington.
Wicks, J. M., and J. C. Bathurst (1996), SHESED: A physically based, distributed erosion and sediment yield component for the SHE hydrological modelling system, *J. Hydrol.*, *175*(1–4), 213–238, doi:10.1016/S0022-1694(96)80012-6.
Wigmosta, M. S., and D. P. Lettenmaier (1999), A comparison of simplified methods for routing topographically driven subsurface flow, *Water Resour. Res.*, *35*(1), 255–264, doi:10.1029/1998WR900017.
Wigmosta, M. S., and L. R. Leung (2001), Potential impacts of climate change on streamflow and flooding in forested basins, in *The Influence of Environmental Change on Geomorphological Hazards in Forested Areas*, edited by R. C. Sidle and M. Chigira, Cent. for Agric. and Biosci. Int., England.
Wigmosta, M. S., and W. A. Perkins (2001), Simulating the effects of forest roads on watershed hydrology, in *Land Use and Watersheds: Human Influence on Hydrology and Geomorphology in Urban and Forest Areas*, edited by M. S. Wigmosta and S. J. Burges, pp. 127–143, AGU, Washington, D. C.
Wigmosta, M. S., L. W. Vail, and D. P. Lettenmaier (1994), A distributed hydrology-vegetation model for complex terrain, *Water Resour. Res.*, *30*(6), 1665–1679, doi:10.1029/94WR00436.
Wigmosta, M. S., B. Nijssen, P. Storck, and D. P. Lettenmaier (2002), The Distributed Hydrology Soil Vegetation Model, in *Mathematical Models of Small Watershed Hydrology and Applications*, pp. 7–42, Water Resour. Publ., Highlands Ranch, Colo.
Wilber, D. H., and D. G. Clarke (2001), Biological effects of suspended sediments: A review of suspended sediment impacts on fish and shellfish with relation to dredging activities in estuaries, *North Am. J. Fish. Manage.*, *21*(4), 855–875, doi:10.1577/1548-8675(2001)021 < 0855:BEOSSA>2.0.CO;2.
Xiao, Y., G. Zhou, and S. Yang (2016), 2D numerical modelling of meandering channel formation, *J. Earth Syst. Sci.*, *125*, 251–267.
Yao, C., and Z. Yang (2009), Parameters optimization on DHSVM model based on a genetic algorithm, *Front. Earth Sci. China*, *3*(3), 374–380, doi:10.1007/s11707-009-0040-6.